國 立 清 華 大 學

碩士論文

脈衝式腔內拉曼鈉黃光雷射

Pulsed Sodium-Yellow Intracavity Raman Laser

系所別 ： 光電工程研究所

學號姓名： 9666505 李傳巽 (Chuan-Hsun Li)

指導教授: 黃衍介 博士 (Dr. Yen-Chieh Huang)

中 華 民 國 九 十 八 年 七 月

Abstract

Recently, high-power and narrow-linewidth sodium-yellow laser generation has been attractive, since it may excite a laser-guide star for the application in adaptive optics, and laboratory spectroscopy. The main purpose of my project is to demonstrate and study the properties of a compact pulsed sodium-yellow intra-cavity Raman laser. Besides, we have proposed some cavity configurations for further narrowing down the linewidth of the output laser. The feasibility and effectiveness of the proposed ideas will be discussed and investigated in the dissertation.

The laser system was fabricated based on a diode-end-pumped Q-switched Nd:YVO_4 laser and stimulated Raman scattering in a Raman crystal $CaWO_4$. We used a fiber-coupled diode laser at 808nm to pump a Nd:YVO_4 crystal. The wave at 1064nm radiated from Nd:YVO_4 could be well confined in a specially designed cavity. By Q-switched operation, a pulse train at 1064 nm with a tunable pulse repetition rate up to 79.4 kHz could be generated to pump an intra-cavity Raman crystal $CaWO_4$. The Raman crystal is used as a wavelength shifter to provide a Raman shift around 910cm^{-1}. Through the stimulated Raman scattering (SRS) in $CaWO_4$, which is a 3rd order nonlinear optical process, a photon of the wave at 1064nm can be transformed into a Stokes photon at 1178nm and an excited optical phonon. Therefore a Raman laser operated at 1178nm is generated. Due to many significant thermal effects in the laser system, the resulted dynamic cavity was modeled and simulated with reference to the actual experiment. The properties and performance of the Raman laser were investigated and studied.

Furthermore, cavities with a grating feedback and an etalon coupler were proposed to narrow down the linewidth of 589nm. Linewidth of around 0.1nm at 1178nm was achieved in a linear cavity configuration with an etalon coupler. Through

the intracavity second harmonic generation (SHG) based on type I noncritical phase matching in a LBO crystal at temperature around 40 degree C, we successfully generated 589nm sodium yellow laser in another linear cavity with yellow-laser power around 360mW, corresponding to a diode-to-yellow-laser conversion efficiency of 2%. On another hand, a folded cavity configuration was proposed for using the grating feedback. The experiment about this part is still under way.

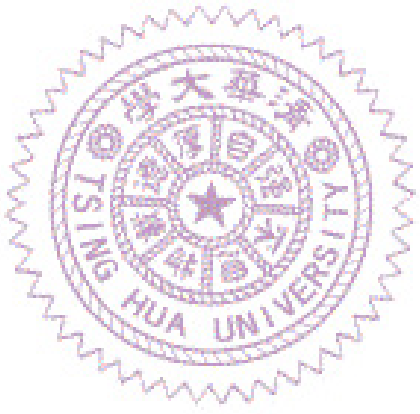

Acknowledgements

I appreciate deeply those who have ever helped and accompanied me during the unforgettable two years in the High-Energy Optics and Electronics Laboratory. Without them, I would not enjoy my graduate life so much. In particular, I would like to give my sincere appreciation to my adviser, Dr. Yen-Chieh Huang, who always encourages and discusses with me patiently. He always stimulates me to think deeply and to realize the physics from another point of view. Additionally, I would like to offer my heartfelt thanks to our group members, Changchih, Tzuhsiang, Chiaying, Yuchung, Yenhou, Grace, Martin, Chiahsian, Vijay, KuanYan, Shoutai, Tsongdong, Yenyin, Yi-Jie, Bing-Kuan, Kunjun, Rongyu, and Hong-Yu. I always treasure our friendship and many pleasant reminiscences of playing basketball, discussion, eating, and chatting. In the end, I am grateful to my parents, younger brother, and May for their continuous cheer and support. They always give me warmness and concern to encourage me to achieve my goal.

Table of Contents

Chapter 1 Introduction

1.1 Motivation

Recently, sodium-yellow laser generation at the sodium D_1 (589.6nm) or D_2 (589nm) line has been attracting people's attention, because a high-power and narrow-linewidth sodium-yellow laser may be utilized to excite a laser-guide star in the mesospheric sodium layer which is 95~105km above the ground for the application in adaptive optics, and laboratory spectroscopy. Refer to Figure 1.1. The general concept is that a high-power, narrow-linewidth sodium-yellow laser on ground can excite the fluorescence of the sodium layer, generating an artificial guide star. The fluorescence image will propagate through the air turbulence between the sodium layer and the ground. People on ground can thus observe and record the image which has been distorted by the air fluctuations. Since the artificial star is far from the ground, the fluorescence image observed on the ground can be regarded as plane wave if there is no turbulence. By comparing and analyzing the images observed on ground with that of the undistorted one, people can know how to correct the distorted image of a distant star which is nearby the guide star.

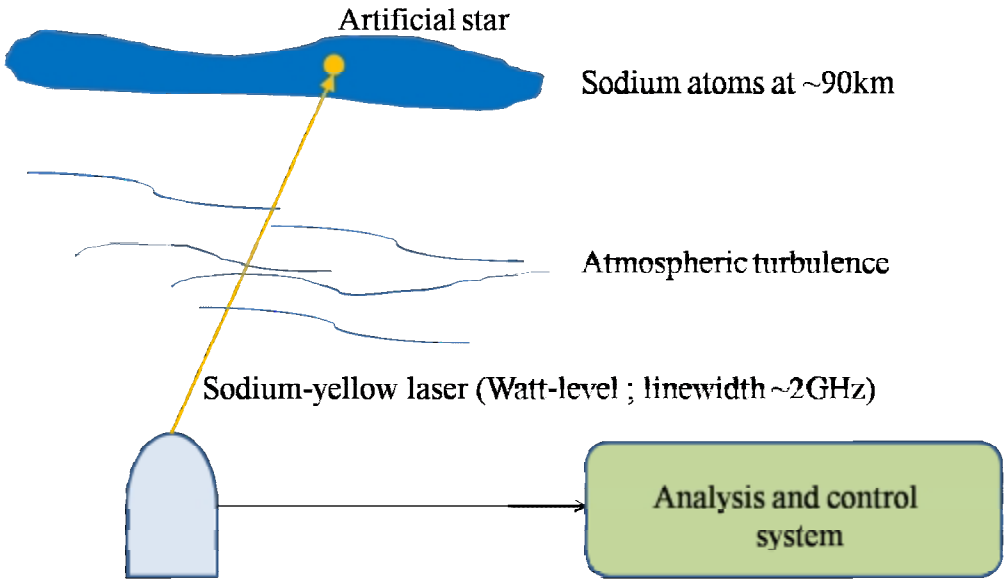

Figure 1.1 An artificial guide star is generated by a high-power, narrow-linewidth sodium-yellow laser on ground for the application in adaptive optics.

There are many people trying to generate sodium-yellow or yellow lasers through different kinds of methods [1~14]. In 1998, James T. Murray et al. [15] reported an end-pumped intracavity solid-state Raman laser that consisted of a Nd:YAG as the gain medium for the laser generation of the fundamental wave at 1064nm, and a Raman crystal, calcium tungstate ($CaWO_4$), as a wavelength shifter for the generation of the first-Stokes wave at 1178nm. After the external-cavity SHG, they successfully generated 250mW sodium-yellow laser at 589nm with efficiency of SHG of 52%, and diode-to-yellow-laser efficiency of 5%. However, since their design was specifically for semiconductor processing applications, the average output power was not enough to generate a laser-guided star; the linewidth of the yellow laser was not characterized and designed. In order to generate artificial guide stars for the application in adaptive optics, the linewidth of the yellow laser has to be within 2 GHz [16], and at least the average output yellow power has to be in watt-level. Therefore, we intended to propose some ideas to improve two main factors, that is, the average power and linewidth of the yellow laser based on the work of James T. Murray et al.; on the other hand, we would like to study and investigate the properties of the modified intracavity $CaWO_4$ Raman laser in detail.

1.2 Diode-End-Pumped Solid-State Laser Systems

Diode-end-pumped solid-state lasers are well-known for the efficiency, compactness, convenience in use and so on [17]. The most common laser gain media

used in this kind of laser system are Neodymium doped vanadate (Nd:YVO_4), Neodymium-doped yttrium aluminum garnet (Nd:YAG), Nd:glass, Nd:YLF and so forth [18]. In particular, Nd:YVO_4 and Nd:YAG are attractive, common, and very important materials because of their high gain, low threshold, good thermal and mechanical properties. They also have high absorption coefficients and broad absorption spectrums which match the laser wavelengths of a number of diode lasers. As a result, end-pumped Nd:YAG and Nd:YVO_4 lasers using diode lasers as the pump source have been very efficient. Furthermore, due to the rapid advancement in the crystal growth, high quality crystals are commercially available. All these advantages make Nd:YVO_4 and Nd:YAG solid-state lasers very useful in a variety of applications such as scientific, industrial, biological and medical researches [19].

In the following, two key points will be introduced: one is the availability of achieving visible laser sources based on Nd:YVO_4 and Nd:YAG solid-state lasers; another one is the significant problems raised by thermal loading that exists intrinsically in these kind of solid-state lasers.

Availability of achieving visible laser sources: Besides those attractive advantages mentioned above, one of the lasing wavelengths of Nd:YVO_4 or Nd:YAG is infrared radiation at 1064nm, making them suitable for generating visible lasers through processes in nonlinear optics. Take Nd:YVO_4 as an example, laser radiation with pump wavelength at 808nm takes place at 1064nm, which corresponds to the transition between energy levels, $^4F_{3/2}(R_1) \rightarrow {}^4I_{11/2}(Y_1)$ [20]. At the first glance, we see that green light at 532nm can be generated by the second harmonic generation (SHG) of 1064nm; most commercial green laser pointers belong to this type of nonlinear process. However, if we want to generate visible lasers with different colors, we must resort to other nonlinear optical mechanisms. Recently, stimulated Raman scattering (SRS) is highly attractive since a Raman medium can provide an

environment for wavelength conversion, resulting in a frequency shift, called the Raman shift, to the incident wave. Furthermore, different Raman media possess different Raman shifts which are independent of the incident wavelength. Therefore, it is wonderful because we can use the common 1064nm laser to generate a new laser source with a longer wavelength, which can be conveniently frequency-doubled to the visible light. In summary, after choosing the proper Raman medium, a new visible laser (even with a desired wavelength) can be achieved through SHG by using a common 1064nm or other infrared laser sources. Thus the coverage of the spectrum in solid-state lasers can then be increased [21]. Details in SRS will be conceptually introduced in the next Section, 1.3, and mathematically described in Section 2.2.

Intrinsic thermal problems: On another hand, when looking into the pump-lasing scheme in Nd:YVO_4 from a "photon" point of view, it is obvious that we have 808nm photons pumping the crystal, generating 1064nm photons. Thus this kind of quantum efficiency will result in thermal heating since excess energy between the 808-nm and 1064-nm photons is generated as heat in the crystal, which will diffuse and result in many thermal problems. In particular, thermal lensing in Nd:YVO_4 will affect the laser system greatly, usually degrading the performance of the laser system due to the resulted cavity instability. Therefore, in order to increase the quantum efficiency in the pumping scheme as well as reduce the thermal heating effect in Nd:YVO_4, people can pump the crystal with a 880nm laser which can be absorbed by Nd:YVO_4 as well, so that the energy difference between 880nm and 1064nm photons is smaller than that with a 808nm pump laser. Hence the quantum efficiency of pumping is increased and the thermal heating is reduced [20]. Furthermore, thermal lensing in the Raman crystal, which results from the inelastic nature of Raman scattering, may also have strong influence on the system stability. The inelastic nature of Raman scattering will be discussed in the next section. In summary, thermal lensing has become a big

problem in the solid-state Raman lasers [18] [21], and it will be discussed in Section 2.6.

1.3 Raman Scattering Process

Spontaneous Raman scattering was first discovered in liquids by Indian physicist Chandrasekhara Venkata Raman in 1928. After a short time stimulated Raman scattering (SRS) was discovered because of the invention of lasers. C.V. Raman was awarded the Nobel Prize for his great work on the scattering of light. Raman scattering has many applications in spectroscopy for material analysis, laser wavelength conversion, advanced solid-state lasers, optical amplification and so on [21] [22] [23].

When the light is scattered by atoms or molecules, a scattered photon usually has the same energy as that of the incident photon, that is, the frequency of the photon is the same before and after the scattering. Refer to Figure1.2 (a), which illustrates the energy levels of a molecule. In this case, a molecule is excited by an incident photon with energy $\mathbf{h}w_p$ from its ground state to a higher virtual energy state. When the molecule goes back to the original ground state, a scattered photon is emitted with the same energy $\mathbf{h}w_p$ as that of the incident photon, meaning that the frequency of the incident wave is the same as that of the scattered wave. This kind of scattering is called elastic scattering or Rayleigh scattering. On the contrary, Raman scattering is a kind of inelastic scattering, meaning that the energy of the scattered photon is different from that of the incident photon. The energy difference usually corresponds to the energy of the vibrational or rotational mode of the host molecule. Refer to Figure 1.2 (b). A photon with energy of $\mathbf{h}w_p$ incident on a crystal excites a molecule

from the ground state to a virtual energy level. Then the molecule does not go back to the original ground state but an intermediate state, depositing energy of $\mathbf{h}w_n$ to a phonon which corresponds to the vibrational mode with frequency w_n of the molecule. Therefore the incident photon has energy exchange with the molecule in the sense that a phonon is excited, having energy of $\mathbf{h}w_n$, and the scattered photon has energy of $\mathbf{h}w_s = \mathbf{h}\left(w_p - w_n\right)$. The scattered photon is called the Stokes wave shown as a orange line in (b), which has frequency of $w_p - w_n$. Note that due to this inelastic nature, heat generated from phonons would be deposited in the Raman crystal, becoming the origin of thermal lensing that will be discussed in Section 2.6. Conceptually speaking, Raman scattering corresponds to the excited "optical phonon", which is associated with localized vibration or rotation. Thus an optical phonon does not have an obvious momentum or have no momentum. From the dispersion curve, that is, the E-k curve of the material (where E is energy and k is the wavevector), an optical phonon is associated with an optical branch. The slope of this branch is horizontal or nearly horizontal, indicating a phonon with no momentum or nearly zero momentum because the slope, dE/dk, is proportional to the momentum of that phonon [24] [25] [26]. Therefore, Raman scattering does not have the requirement of phase matching or it is automatically phase-matched. As we will see in Chapter 2, many other nonlinear processes, such as SHG, SFG and so on, need to be phase-matched. This means that an environment is created such that momentum is conserved for the desirable process. On the other hand, Brillouin scattering corresponds to the excited "acoustic phonon", which is associated with the acoustic branch in the dispersion curve. This kind of phonon, on the contrary, possesses a momentum. From the acoustic branch of the dispersion curve, it is clear that the slope of the branch is

obvious and thus the momentum of a phonon is not zero.

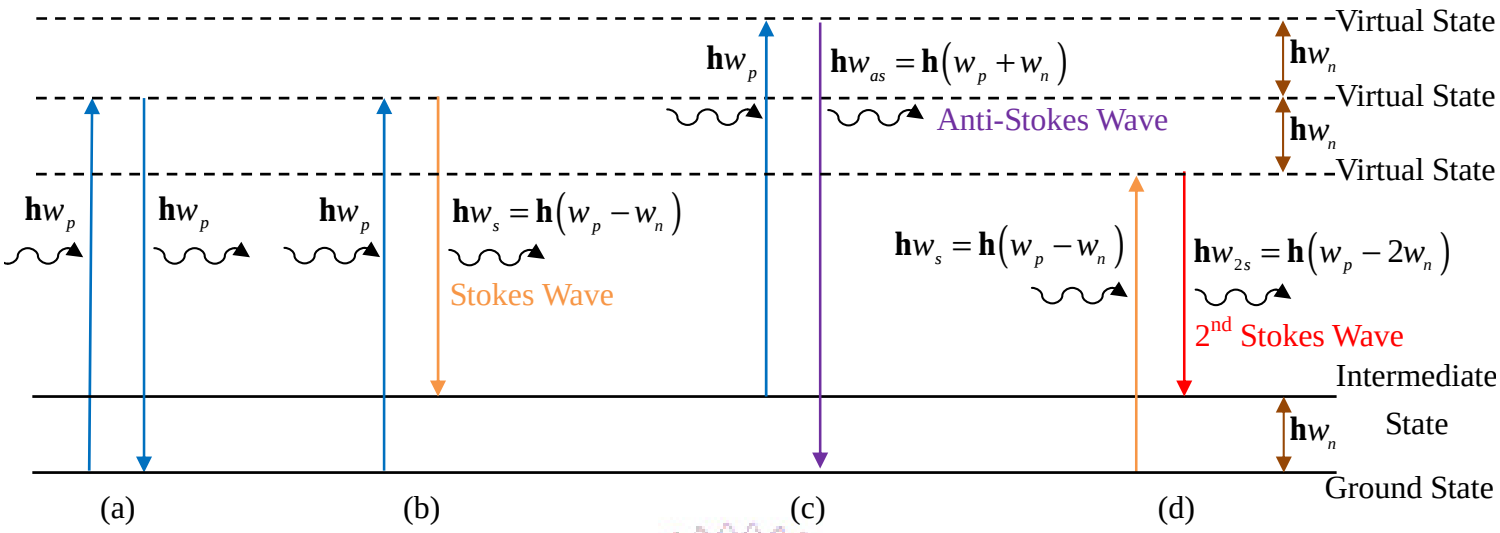

Figure 1.2 Energy-level diagram of a molecule. (a) Elastic scattering or Rayleigh scattering: the incident photon does not have energy exchange with the molecule. The scattered photon has the same energy as that of the incident photon. The frequency of the incident wave is the same as that of the scattered wave. (b) Generation of the Stokes wave in Raman scattering: the incident photon deposits energy of $\hbar w_n$ to the molecule to excite the optical phonon of a vibrational mode in a crystal. The scattered photon thus has energy of $\hbar w_s = \hbar(w_p - w_n)$ and frequency of $w_p - w_n$. (c) Generation of the anti-Stokes wave in the Raman scattering: When the pump wave possessing photon energy of $\hbar w_p$ is strong enough such that the intermediate state is populated, there is some possibility for the incident wave to directly pump the molecules at the intermediate state to the higher virtual energy level. When the molecule at the virtual state goes back to the original ground state, the optical phonon loses energy of $\hbar w_n$, and the anti-Stokes wave with photon energy of $\hbar w_{as} = \hbar(w_p + w_n)$ is generated significantly. For this case to happen, higher pump power is needed. (d) Generation of the second Stokes wave: when the first Stokes wave is strong enough and behaves as a pump wave to excite the molecule at the ground state to a virtual state, there is possibility for the molecule to lose energy of $\hbar w_n$, exciting an optical phonon so that the emitted photon has energy of $\hbar w_{2s} = \hbar(w_p - 2w_n)$.

When the pump wave is strong enough, Raman scattering can become SRS, just like the stimulated emission for coherent light amplification. This is because there are

many molecules at the higher virtual energy level and many photons of the spontaneous Stokes wave. (Strictly speaking, all emission processes are stimulated emission according to QED (Quantum Electrodynamics), since the so-called spontaneous emission is stimulated by vacuum noise, which exists even at 0 Kelvin temperature.) When the first Stokes wave is strong enough or comparable to the incident wave, it can behave like a pump wave to excite molecules at the ground state to a virtual energy state. Refer to Figure 1.2 (d), the orange line representing the incident wave or pump wave is the Stokes wave, which is also shown in (b) by the same color. There is possibility for molecules at the virtual state in (d) to go to the intermediate state and lose energy $\mathbf{h}w_n$ to excite the optical phonons. This is also a Raman scattering process. Now the scattered photon is called the second Stokes wave, possessing energy $\mathbf{h}w_{2s} = \mathbf{h}\left(w_p - 2w_n\right)$ shown as a red line in (d). Similarly, the generation of the third Stokes wave is possible, if the second Stokes wave is strong enough to pump the molecules and so forth. Another interesting possible phenomenon is that there is also possibility for the incident photon with energy of $\mathbf{h}w_p$, shown as a blue line in (a) (b) (c), to directly pump the molecule at the intermediate state which corresponds to the vibrational mode to a virtual energy level. Refer to Figure 1.2 (c), when the molecule goes back to the original ground state, the optical phonon actually loses energy of $\mathbf{h}w_n$ so that the emitted photon has energy of $\mathbf{h}w_{as} = \mathbf{h}\left(w_p + w_n\right)$ or frequency of $w_p + w_n$. It is called the anti-Stokes wave shown as a purple line in (c). However, the anti-Stokes wave is significant only when the intermediate state is populated. This means that the pump wave possessing photon energy of $\mathbf{h}w_p$ has to be strong enough such that the first Stokes wave is significant or the number of molecules at the intermediate state is significant. Hence the generation of the

anti-Stokes wave usually needs higher pump power.

It is also possible to see multiple peaks simultaneously on the spectrum which includes the fundamental pump wave, the Stokes wave, the second Stokes wave, higher-order Stokes waves or even the anti-Stokes wave.

In summary, Raman scattering is an inelastic scattering, resulting in the thermal lensing effect in a Raman crystal naturally. It is usually a frequency down-conversion process like the generation of the first Stokes wave and second Stokes wave in Figure 1.2 (b) and (d), respectively. It is rarely a frequency up-conversion process like the generation of the anti-Stokes wave in Figure 1.2 (c).

Therefore, this effect can be used in laser systems to generate laser sources at new wavelengths.

1.4 Possible Configurations of Raman Lasers

Based on the concept for fabricating laser sources at new wavelengths by taking advantage of the SRS, there are many possible basic configurations for solid-state Raman lasers that will be introduced later. If people are interested in Raman lasers that emit at only one wavelength, usually at the first Stokes wavelength, then only the first Stokes wave is concerned and the laser cavity is designed carefully for the fundamental wave and the first Stokes wave. Additionally, it is better if the generation of other high-order Stokes waves is avoided, since it is a type of loss for degrading the growth of the first Stokes wave. In the following, we concern only the first Stokes wave.

In some cases, a crystal can be the laser gain medium for the fundamental wave as well as the Raman active medium for the Stokes wave, if having a high Raman gain coefficient. Hence it is possible to achieve a self-Raman laser in which a crystal

plays both roles simultaneously. In this kind of system, when the fundamental wave is generated, it can further generate the Stokes wave through SRS in the same crystal. However, the thermal heat generated during the pumping process together with the heat resulted from the inelastic nature of Raman scattering may produce severe thermal loading on the same crystal. Thus usually the cavity should be designed more carefully and good cooling systems are needed [21].

In the following, we consider the case where two different crystals acting as gain media for the fundamental wave and the first Stokes wave, respectively. There are basically three possible configurations for consideration [21]:

1. External Raman resonator:

Refer to Figure 1.3, the Raman crystal is placed inside a resonator formed by M1 and M2, being pumped by a pump laser outside the resonator, where the pump laser is the fundamental wave. M1 is preferred to have high transmittance at the pump wavelength but high reflectivity at the first Stokes wavelength. M2 is preferred to have high reflectivity at the pump wavelength and have designed transmittance to optimize the Raman laser output. Thus, typically the pump laser can pass the Raman crystal at least twice so that the threshold for Raman laser generation would be lower than that in the single-pass Raman generator. On another hand, the beam quality of the Raman laser output may also be improved compared to the Raman generator because of the designed resonator mode. However, more attention should be paid on the mode-matching between the pump laser mode and the resonator mode as well as the possible thermal lensing effect in the Raman crystal. The coupling lens set in the figure as well as the two mirrors are designed to achieve good mode-matching.

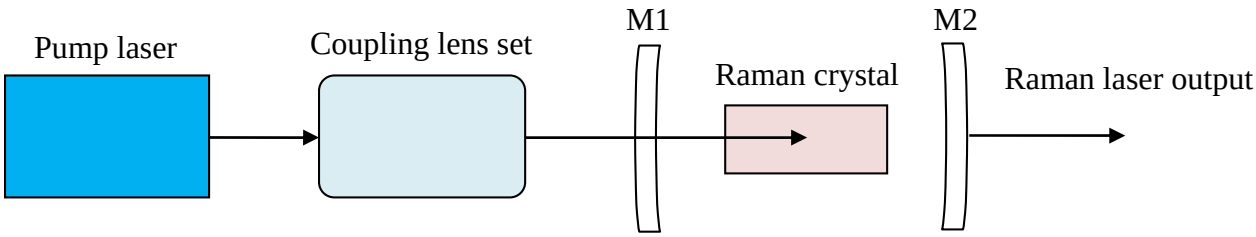

Figure 1.3 The illustration of an external Raman resonator. The threshold of the Raman laser is lower and the beam quality may be improved in comparison with the single-pass Raman generator. The cavity needs to be designed carefully. More attention should be paid on the mode-matching between the pump laser mode and the resonator mode as well as the possible thermal lensing effect in the Raman crystal.

2. Intracavity Raman laser:

The main difference between a intracavity Raman laser and an external Raman resonator is that the Raman crystal is placed inside the cavity of the fundamental wave. This means that the higher intracavity power density can be utilized to pump the Raman crystal, resulting in a lower Raman threshold. Besides, multiple round trips of the fundamental wave inside the cavity can further increase the effective interaction length of the Raman crystal. Therefore we intend to choose this configuration for our Raman laser.

Refer to Figure 1.4, typically this kind of configuration takes advantage of the diode-end-pumped laser system as emphasized in Section 1.2. A diode laser will pump the laser crystal inside the cavity formed by M1 and M2, generating laser at the fundamental wavelength. Through Q-switched operation, the pulse train of the fundamental wave is obtained and oscillates in the cavity. The two mirrors are preferred to have high reflectivity at the fundamental wavelength such that the fundamental wave can be confined well in the cavity so as to have good interaction with the Raman crystal. The high peak power of each pulse will lower the Raman

threshold substantially in comparison with that in the CW operation, as will be explained in Section 2.2. This is the reason that we have chosen the pulsed operation for our Raman laser. Additionally, the Raman laser output can be optimized by choosing the two mirrors with proper coatings at the Stokes wavelength. M1 and M2 thus are said to form a shared cavity, in which lasers at two different wavelengths oscillate simultaneously.

In order to generate a sodium-yellow laser, SHG process is necessary. This part is left to Section 2.3 for detailed explanation.

Additionally, CW Raman lasers have been designed and developed since 2004. Because of the advantages of the intracavity configuration, CW Raman laser may be realized without the Q-switch in Figure 1.4 [7] [27] [28], depending on many factors that are beyond the scope of and will not be discussed in this dissertation. However, CW Raman lasers actually have many similar design principles to pulsed ones, such as dealing with thermal lensing and cavity design for good energy transfers. The detailed design and parameters are addressed in Chapter 3.

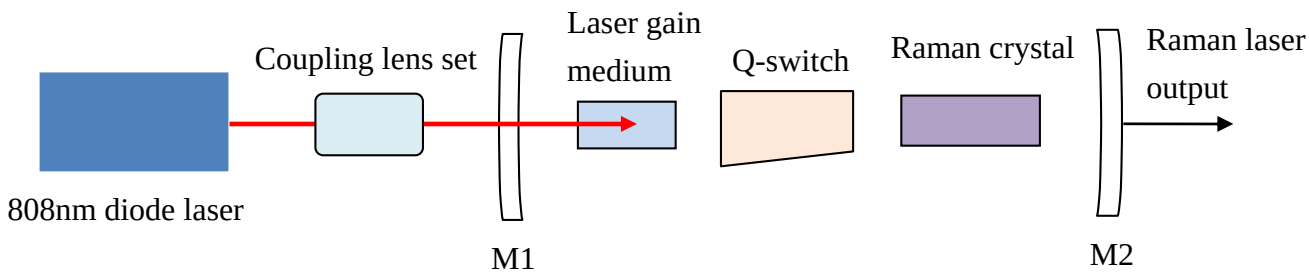

Figure 1.4 The illustration of an intracavity Raman laser. The Raman crystal is placed inside the cavity of the fundamental wave. Thus the higher intracavity power density can be utilized to pump the Raman crystal, resulting in a lower Raman threshold. Besides, multiple round trips of the fundamental wave inside the cavity can further increase the effective interaction length of the Raman crystal. By Q-switched operation, the high peak power of each pulse will lower the Raman threshold substantially in comparison with that in the CW operation.

1.5 Overview of the Dissertation

In this chapter, the diode-end-pumped solid-state laser system and Raman scattering have been introduced conceptually. Then, the combination of them, that is, the aspect of the diode-end-pumped solid-state Raman laser was introduced. Several considerations from other people's work in this kind of Raman lasers were also reviewed. Based on this introductory chapter, some mathematical treatment or more detailed concepts of the physical mechanisms in Raman lasers will be addressed in Chapter 2. The detailed design and parameters of our experiments will be reported in Chapter 3. The experimental results, conclusions, and comparisons will also be discussed in Chapter 3. The future work and final conclusions will be left to Chapter 4.

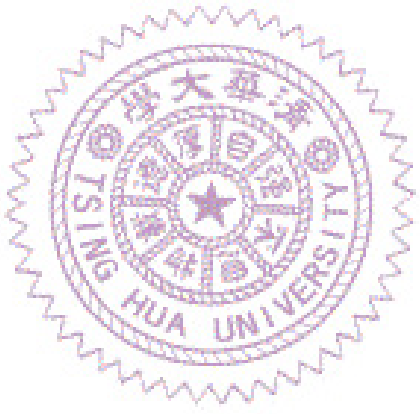

Chapter 2 Physical Mechanisms in Our Raman Laser

2.1 Diode-End-Pumped Q-Switched Nd:YVO_4 Laser Generation

We have introduced the diode-end-pumped solid-state laser system and the diode-end-pumped Raman laser system in Section 1.2, 1.3, and 1.4. The pulsed intracavity Raman laser without the Raman crystal is actually a basic diode-end-pumped Q-switched solid-state laser. The Q-switched operation is a kind of method to transform a CW laser into a pulsed one. By using a RF driver together with a function generator, people can feed a desirable RF signal into the Q-switch crystal, such as a crystal quartz, to modify its refractive index. The crystal will behave as an acousto-grating so that the incident electromagnetic wave will be diffracted according to the law of Bragg diffraction. In this way, a periodic RF signal generated from the function generator can thus modify the refractive index such that in a period of the RF signal, the crystal acts as a grating for most of time, and becomes a normal crystal for the rest short time. During the period of time when the crystal acts as a grating, great loss will be introduced to the laser system, and the pump energy is accumulated in the form of population inversion since lasing is prohibited. When the crystal becomes normal, a pulse is formed within the short period of time. Due to the periodic operation, a pulse train is formed. The pulse repetition rate of the pulse train can be controlled by the RF signal.

Because the fluorescence lifetime of Nd:YVO_4 is relatively short compared with that of Nd:YAG, usually a Q-switched Nd:YVO_4 laser needs to be operated at relatively high pulse repetition rate such that the average output power close to CW performance can be achieved [20]. Therefore, we expect that the operated pulse repetition rate in our Raman laser system will be higher than that in the laser built up

by James T. Murray et al in [15].

In the following, mathematical derivations are mainly referred to [24] and [29].

2.2 Stimulated Raman Scattering (SRS) in Calcium Tungstate ($CaWO_4$)

In order to extract the energy, for example, from one wavelength to another wavelength by using principles in nonlinear optics, we have to resort to Maxwell equations to see what would happen for a given nonlinear optical process with initial conditions. Understanding the physical mechanisms behind a phenomenon will let us realize the key parameters or factors, helping us in designing and doing the experiment.

To explain the physical meaning of Raman scattering and express it in terms of mathematics, let us start from Maxwell equations:

$$\nabla \times \vec{E} = -\frac{\partial \vec{B}}{\partial t} \quad \text{and} \quad \nabla \times \vec{H} = -\frac{\partial \vec{D}}{\partial t} \tag{1}$$

where $\vec{D} = e_0 \vec{E} + \vec{P} = e_0 \vec{E} + \left(\vec{P}_L + \vec{P}_{NL}\right) = e_0 \ddot{e}_r \vec{E} + \vec{P}_{NL}$

In the above equation, $\vec{P}$ is the total polarization vector, which is the combination of the linear term, $\vec{P}_L$, and the nonlinear polarization, $\vec{P}_{NL}$, where $\vec{P}_L$ is in proportion to the electric field intensity, $\vec{E}$, and $\vec{P}_{NL}$ is a power series of the square and higher orders of $\vec{E}$; $\vec{B}$ is magnetic flux density; $\vec{H}$ is magnetic field intensity; $\vec{D}$ is electric displacement; t is time; e_0 is vacuum permittivity; $\ddot{e}_r$ is relative permittivity tensor. Combining the equations in (1), we get the following wave equation for the radiation field $\vec{E}$:

$$\nabla^2 \vec{E} - \frac{\ddot{e}_r}{c_0^2} \frac{\partial^2 \vec{E}}{\partial t^2} = m_0 \frac{\partial^2 \vec{P}_{NL}}{\partial t^2}$$

The right-hand-side of the equation acts as a driving term for $\vec{E}$.

Assume the electromagnetic wave is a plane wave propagating along z direction, that is, $\vec{\vec{E}}(z,t)=\frac{1}{2}\left[\vec{\bar{E}}(z,w)e^{j(wt-\vec{k}\cdot\vec{z})}+c.c.\right]=\frac{1}{2}\left[\vec{\hat{E}}(z,w)e^{jwt}+c.c.\right]$, where "$\rightarrow$" atop a letter means a vector; "~" atop a letter means a real quantity; "-" atop a letter means the field envelope; "^" atop a letter means a phasor; c.c. means the complex conjugate of the previous terms; k is the wave vector; w is the angular frequency of the field. Under slowly varying envelope approximation (SVEA), that is, $\left|\frac{\partial^2\vec{\bar{E}}}{\partial z^2}\right|<<\left|k\frac{\partial\vec{\bar{E}}}{\partial z}\right|$, meaning that the variation of the field envelope along z is fairly slower than the oscillation of the field, we can get the following governing equation which can describe all nonlinear optical processes provided that the above assumption is valid:

$$\frac{\partial\vec{\bar{E}}(z,w)}{\partial z}=-j\frac{m_0c_0w}{2n_w}\vec{\hat{P}}_{NL}(z,w)e^{j\vec{k}\cdot\vec{z}} \tag{2}$$

where m_0 is vacuum permeability, c_0 is the velocity of light in vacuum, and n_w is the refractive index at w. Equation (2) means that the nonlinear polarization vector of angular frequency w forces an electromagnetic wave of the same angular frequency, w.

Raman scattering is a third-order nonlinear optical process in which the multiplication of three electric fields manipulated by the third-order susceptibility drives the dipole oscillation in the material to generate the fourth wave. Hence it is also called four-wave mixing. Brillouin scattering, self-focusing, third harmonic generation and so on are also third-order nonlinear optical phenomena. To investigate the development of and interaction between frequency components, it is intended to write the phasor of the nonlinear polarization, $\hat{P}_{NL}(z,w_s)$ at frequency w_s, in terms of the three driving electric fields at frequencies w_1, w_2, and w_3, respectively. It is therefore in the form of the following equation in which $c_{eff}^{(3)}$ is the effective

third-order susceptibility resulted from considering contributions from multiplications of various combinations of components of three electric fields along different directions:

$$\hat{P}_{NL}(z,w_s) = e_0 c_{eff}^{(3)} \bar{E}(w_1)\bar{E}(w_2)\bar{E}(w_3) e^{-j(\vec{k}_1+\vec{k}_2+\vec{k}_3)\cdot\vec{z}} \tag{3}$$

where $w_s = w_1 + w_2 + w_3$. Thus equation (2) becomes

$$\frac{\partial \bar{E}(z,w_s)}{\partial z} = -j\frac{w_s}{2c_0 n_{w_s}} c_{eff}^{(3)} \bar{E}(w_1)\bar{E}(w_2)\bar{E}(w_3) e^{-j\Delta\vec{k}\cdot\vec{z}} \tag{4}$$

where $\Delta\vec{k} = \vec{k}_1 + \vec{k}_2 + \vec{k}_3 - \vec{k}_s$.

Notice that from the mathematics point of view, the frequencies w_1, w_2, and w_3 shown in equation (4) can be "negative frequencies", implying many possibilities of combinations in $w_s = w_1 + w_2 + w_3$. It indicates that there are many possible ways to generate the fourth wave at frequency w_s. Based on the introduction in Chapter 1, there are actually only two photons at different frequencies, w_s and w_p, respectively, participating in the stimulated Raman scattering process. Therefore the only possible way to generate the fourth wave at w_s in the SRS process is $w_s = w_s + w_p - w_p$, corresponding to three waves at frequencies w_s, w_p, and $-w_p$, respectively. Likewise, the only possible combination of three waves to generate the fourth wave at w_p is $w_p = w_p + w_s - w_s$.

Assume collinear interaction along z; take the case in which the fourth wave at w_s is generated for an example. Note that the phasor of the electric field at $-w_p$ in the involving three waves is $\hat{E}(z,-w_p) = \bar{E}(-w_P)e^{-jk_p z}$. Since the electric field at w_p in the real world is represented by the real quantity $\tilde{E}(z,t)$, where

$$\bar{E}(z,t)=\frac{1}{2}\left[\hat{E}(z,w_p)e^{jw_pt}+\hat{E}^*(z,w_p)e^{-jw_pt}\right]=\frac{1}{2}\left[\hat{E}(z,w_p)e^{jw_pt}+\hat{E}(z,-w_p)e^{j(-w_p)t}\right].$$

Thus the relation $\bar{E}(-w_p)=\bar{E}^*(w_p)$ holds. Similarly, $\bar{E}(-w_s)=\bar{E}^*(w_s)$ holds. Therefore, from equation (4), we can get the two coupled wave equations:

$$\frac{\partial\bar{E}_p(z,w_p)}{\partial z}=-j\frac{w_p}{2c_0n_{w_p}}c_{eff}^{(3)}\bar{E}_p(w_p)\left|\bar{E}_s(w_s)\right|^2 \tag{5}$$

$$\frac{\partial\bar{E}_s(z,w_s)}{\partial z}=-j\frac{w_s}{2c_0n_{w_s}}c_{eff}^{(3)}\bar{E}_s(w_s)\left|\bar{E}_p(w_p)\right|^2 \tag{6}$$

where $\Delta k=k_p+k_s-k_s-k_p=0$ in (5), and $\Delta k=k_s+k_p-k_p-k_s=0$ in (6).

Note from equation (5) and (6) that the forward Raman scattering process does not have a phase matching condition. That is, we do not have to build up a proper environment specifically for momentum conservation in this given process. The physical reason has been addressed in Chapter 1. Furthermore, equation (5) and (6) describe the development of the pump wave and the first Stokes wave, respectively. Observe that if $c_{eff}^{(3)}$ is real, then the pump wave or the Stokes wave just experience a phase shift modulated by the intensity of the other one. If $c_{eff}^{(3)}$ is purely imaginary, this means that the molecular is at resonance and the material has absorption of the incident wave. From equation (6), we can see that the electric field of the first Stokes wave thus has an exponential gain in which the exponent contains the intensity of the pump wave. This is consistent with the concepts in Chapter 1 in the sense that the molecule absorbs partial energy of the pump photon to excite a phonon of a vibrational mode.

By using $\frac{dI}{dz}=\frac{1}{2Z}\left(E^*\frac{dE}{dz}+E\frac{dE^*}{dz}\right)$ to rewrite equation (5) and (6), where *I* is the intensity and Z is the wave impedance in the medium, we have

$$\frac{\partial I_{w_p}}{\partial z} = -\frac{w_p}{w_s} d_s I_{w_p} I_{w_s} \quad \text{and} \quad \frac{\partial I_{w_s}}{\partial z} = d_s I_{w_p} I_{w_s}$$

where d_s is defined to be: $d_s = \frac{2w_s \operatorname{Im}\left(c_{eff}^{(3)}\right)}{n_{w_s} n_{w_p} c_0^2 e_0}$ which is called the Raman gain coefficient with common units in cm/GW, I_{w_s} is the intensity of the Stokes wave, and I_{w_p} is the intensity of the fundamental wave. Additionally, the photon numbers are conserved in Raman scattering process, so the relation

$$\frac{I_{w_s}(z)}{w_s} + \frac{I_{w_p}(z)}{w_p} = \frac{I_{w_s}(0)}{w_s} + \frac{I_{w_p}(0)}{w_p} = K$$

holds, meaning that the total number of the pump photons and Stokes photons remain the same. Therefore the following expressions are obtained:

$$I_{w_s}(z) = \frac{Kw_s}{1 + \frac{w_s}{w_p}\frac{I_{w_p}(0)}{I_{w_s}(0)} e^{-d_s w_p K z}} \quad \text{and} \quad I_{w_p}(z) = \frac{Kw_p}{1 + \frac{w_p}{w_s}\frac{I_{w_s}(0)}{I_{w_p}(0)} e^{d_s w_p K z}}$$

From above equations we can see that the energy will be extracted from the pump wave to the first Stokes wave when the pump wave propagates along z if d_s is positive. The Stokes wave will grow up at the expense of the pump wave.

For simplicity, assume that the pump wave does not change a lot while propagating along z. Under this low conversion efficiency assumption, the intensity of the Stokes wave at z becomes:

$$I_{w_s}(z) = I_{w_s}(0) e^{g_s z} = I_{w_s}(0) e^{d_s I_{w_p}(0) z}$$

This means that the intensity at z is proportional to an exponential gain in which the exponent is the multiplication of the Raman gain coefficient d_s, the initial pump intensity $I_{w_p}(0)$ at z=0, and the propagating distance z.

Conclusion: there is large gain for the Stokes wave if people can find a material with a

large Raman gain coefficient d_s, have a pump laser with strong intensity incident on that material, and have long material length for propagation. This is the reason that we choose an intracavity Raman laser configuration because very high intensity of the pump wave in the cavity can be utilized.

In order to make the Stokes wave oscillate in the cavity, the total gain has to be greater than the total loss at the Stokes wavelength. The threshold condition for a Raman laser is given by

$$R_1 R_2 e^{d_s I_{wp}(0) 2l - a_s 2L} \geq 1 \tag{7}$$

where R_1, R_2 are the power reflectances of the two cavity mirrors at the first Stokes wavelength, a_s is the effective distributed power attenuation coefficient of the cavity at the first Stokes wavelength, 2L is the round-trip length of the cavity, and *l* is the crystal length.

Note that from discussions in Chapter 1 and Section 2.2, the First Stokes wavelength can be tuned by changing the wavelength of the pump laser.

It is important to note that the directional relation between the polarization of the pump laser, the propagating direction of the laser beam, and the crystal orientation, because different relations may indicate different ways of interaction between light and matter, resulting in different Raman gain coefficients. For example, the laser may see different crystal structures and force the molecules to oscillate in different ways. In Calcium Tungstate, $CaWO_4$, the configuration which provides the Stokes wave with the largest Raman gain coefficient is that the polarization of the pump laser, the direction of the laser beam, and the crystal axis are perpendicular to one another [30]. In this kind of interaction, the Raman gain coefficient was calculated to be 1.1cm/GW at l064nm [30].

There are many papers reporting material properties of $CaWO_4$ [21] [30] [31]. In

particular, the Raman shift is about 910cm^{-1} and the linewidth is measured to be 7.0 cm^{-1} in [30]. Therefore the first Stokes wavelength pumped by 1064nm laser is around 1178nm. The sodium-yellow laser radiation is generated through SHG process of 1178nm. This is the reason that we chose $CaWO_4$ as a Raman shifter for our intracavity Raman laser. Additionally, from the spontaneous Raman spectrum in [21], we see that there are two Raman peaks: the most intense one corresponds to 910cm^{-1}, the other weaker one corresponds to around 333cm^{-1}, which was calculated from the experimental results in which a signal centered at 1103.5nm was observed in our experiment. It will be reported in Chapter 3.

Some material properties of $CaWO_4$ are summarized in Table 2.1:

Table 2.1 Material properties of $CaWO_4$

Transmission Range (mm)	0.2-5.3 [32]
Refractive Index (at 300K)	1.884(o), 1.898(e) [32]
Density (g/cm)	6.116 [32], insoluble in water
Crystal Symmetry	Tetragonal [32]
Raman Shift at 300K (cm^{-1})	~910 [30], 910.7 [33]
Spontaneous Raman Linewidth (cm^{-1})	7.0 [30], 4.8 [34]
Optical Damage Threshold (MW cm^{-2})	500
Raman Gain Coefficient with 1064nm Pump (cm/GW)	1.1 [30]
Calculated values by assuming that 1W Stokes photons are generated with 200 mm mode size in the Raman crystal which has transverse area of 5x5mm^2 [21]	
Calculated Thermal Time Constant (s)	0.95 [21]
Calculated Thermal Lens (m)	-1.8 [21]

Thermal Conductivity (W m^{-1} K^{-1}) at $25\,^{o}C$	16 [32]
dn/dT (10^{-6})	-7.1(o), -10.2(e) [32]
Heat capacity (J/gK)	0.396 [32]

2.3 Intracavity and Extracavity Second Harmonic Generation (SHG) in Lithium Triborate (LBO, LiB_3O_5)

Second harmonic generation (SHG) is a second-order nonlinear optical process in which two photons with the same frequency w generate one photon with frequency $2w$. This is an easier process because the second harmonic photon originates from two existing photons. The mathematical treatment of SHG is similar to Raman scattering: do analysis from the governing equation (2) in Section 2.2, and then discuss the phase matching condition and the related important physical parameters.

The two coupled wave equations (8) and (9) shown below for the fundamental wave and the second harmonic wave are similar to (5) and (6) in Section 2.2. Main differences are: Δk is not automatically zero, meaning that a phase matching condition exists; the nonlinear coefficient is the second order one, d_{eff}, rather than $c_{eff}^{(3)}$; the process is three-wave mixing, and thus the right-hand-side of the equation includes multiplication of two electric fields, rather than three. Assume $n \approx n_w \approx n_{2w}$, we get

$$\frac{d\bar{E}_{2w}}{dz} = -jk\,\bar{E}_w^2 e^{j\Delta\vec{k}\cdot\vec{z}} \tag{8}$$

$$\frac{d\bar{E}_{w}}{dz} = -jk\,\bar{E}_{2w}\bar{E}_w^{*} e^{-j\Delta\vec{k}\cdot\vec{z}} \tag{9}$$

where $k \equiv \frac{d_{eff} w}{c_0 n}$, and $\Delta \vec{k} = \vec{k}_{2w} - 2\vec{k}_w$

Assume the fundamental wave and the second harmonic wave propagate along the z direction. Then we have the collinear phase matching condition $\Delta \vec{k} \cdot \vec{z} = 0$ or $\Delta k = k_{2w} - 2k_w = 0$. This means that $n_w = n_{2w}$.

Under non-depleted pump condition and $\Delta k = 0$, the solutions for two coupled wave equations can be solved easily. It is found that:

$$I_{2w}(z) \approx 2Zk^2 I_w^2(0) z^2 \propto \frac{d_{eff}^2}{n^3} z^2 \qquad (10)$$

where $I_{2w}(z)$ is the SHG intensity after propagating a distance z.

Conclusion: from (10) it is found that a long crystal and large d_{eff} is preferred. Note that this condition holds without considering problems related to walk-off angle and walk-off time in the pulsed scheme.

In our experiment, we chose Lithium Triborate (LiB_3O_5 or LBO) as the SHG crystal. It has several advantages such as broad transparency range from 160nm to 2600nm, larger nonlinear coefficient than that of KDP by three times, and wide wavelength range for operated in type I and type II noncritical phase matching (NCPM) [35]. In order to achieve the phase matching condition of a SHG process in LBO, typically angle phase matching or NCPM is the possible way. In particular, we intend to do SHG process with NCPM to ease the difficulty in alignment of LBO in the cavity. The following Table 2.2 summarizes some material properties of LBO [35] [36]:

Table 2.2 Some material properties of LBO

Crystal Structure	Orthorhombic, point group mm2, space group $Pna2_1$
Optical Symmetry	Negative biaxial

Density	$2.47 g/cm^2$
Lattice Parameter	a=8.4473 $\mathring{A}$, b=7.3788 $\mathring{A}$, c=5.1395 $\mathring{A}$, Z=2
Melting Point	~834 ^oC
Mohs Hardness	6
Thermal Conductivity	3.5W/m/K
Nonlinear Coefficient	$d_{eff}(I) = d_{32}\cos j$ $d_{eff}(I) = d_{31}\cos^2 q + d_{32}\sin^2 q$ $d_{eff}(II) = d_{31}\cos j$ $d_{eff}(II) = d_{31}\cos^2 q + d_{32}\sin^2 q$ $d_{31} = (1.09 \pm 0.09)\ pm/V$ $d_{32} = (1.17 \pm 0.14)\ pm/V$
Sellmeier Equations (l in mm)	$n_x^2 = 2.454140 + 0.011249/(l^2 - 0.011350) - 0.014591 l^2 - 6.60\times10^{-5} l^4$ $n_y^2 = 2.539070 + 0.012711/(l^2 - 0.012523) - 0.018540 l^2 + 2.0\times10^{-4} l^4$ $n_z^2 = 2.586179 + 0.013099/(l^2 - 0.011893) - 0.017968 l^2 - 2.26\times10^{-4} l^4$
Refractive Indices	n_x= 1.5656, n_y=1.5905, n_z=1.6055 at 1064nm
NCPM SHG Temperature Dependence (T in ^oC , l in mm)	
Type I : 950~1300nm	$T_1 = -1893.3 l^4 + 8886.6 l^3 - 13019.8 l^2 + 5401.5 l + 863.9$
Type I : 1300~1800nm	$T_2 = 878.1 l^4 - 6954.5 l^3 + 20734.2 l^2 - 26378 l + 12020$
Type II : 1100~1500nm	$T_3 = -21630.6 l^4 + 112251 l^3 - 220460 l^2 + 194153 l - 64614.5$
Damage Threshold TEM_{00} Mode at 1064nm	>10GW/cm^2 at 10ns

NCPM process is relatively insensitive to the incident angle of the pump laser compared with the angle phase matching. In LBO, it is achieved by tuning the crystal

temperature such that the phase matching condition $n_w = n_{2w}$ is satisfied when the laser propagates along the crystal x axis in type I NCPM.

According to the formulas for type I and type II NCPM SHG temperature shown in Table 2.2, we can draw the following Figure 2.1 for the NCPM temperature with respect to the fundamental wavelength. We chose type I NCPM in our experiment in which the laser beam propagated along the crystal x axis. The type I NCPM temperature for fundamental wavelengths at 1064nm and 1178nm are calculated to be $149.26\,^{o}C$ and $40.49\,^{o}C$, respectively. There is one paper reporting the measured NCPM temperature for SHG of 1178nm, which is around $40\,^{o}C$ [12].

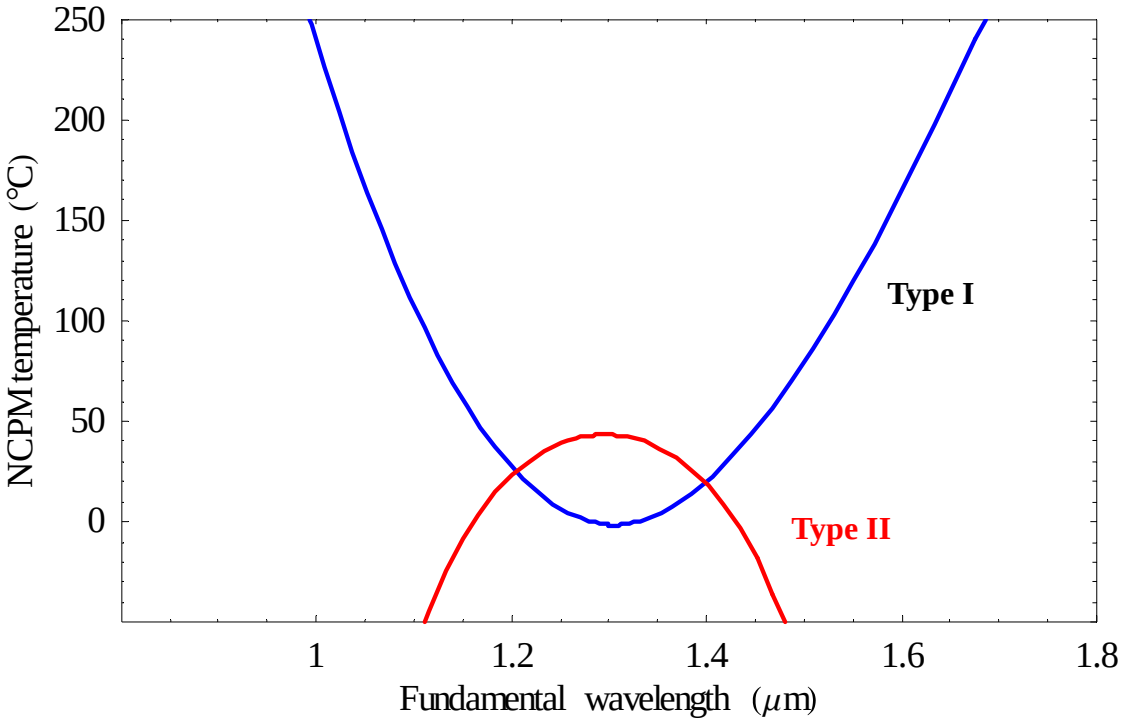

Figure 2.1 Type I and type II NCPM temperature (^{o}C) versus the fundamental wavelength (mm)

The coating specifications of our LBO are:

AR: Anti-Reflection

AR coating on both faces	R<0.3%@1178nm & 1064nm ; R<0.5%@589nm

Table 2.3 AR coating specifications of our LBO

Basically, there are two ways that can be adopted to get the second harmonic of the Stokes wave: the extracavity or intracavity SHG. As for the extracavity SHG, the nonlinear crystal for SHG is placed outside the cavity. Therefore the coating on M2 needs to be designed such that the output Raman laser is optimized to be the input of the SHG process. As for the intracavity SHG which utilizing the high intracavity power, the coating on M2 needs to be high reflective at both the fundamental and first Stokes wave such that they are confined well in the shared cavity. However, more attention should be paid in this configuration because the insertion of the SHG crystal will change the original cavity modes. Besides, it also increases the net cavity length and may cause the cavity become unstable easily in high-power operation. Therefore it raises the difficulty in the cavity design. The system should be carefully designed to provide the most efficient energy transfers in optical processes.

Another point is that we can focus the laser beam at our will to pump the SHG crystal below the damage threshold. However, limitations appear when placing SHG crystal inside the cavity. The pump beam size is limited to be the cavity mode size. Although we can increase the cavity length to make the cavity mode size become small, the intracavity power may not increase or even decrease due to the resulted cavity instability raised by thermal loading.

It is therefore obvious that the thermal problem should be considered carefully in the cavity design since it always exists and affects the cavity mode greatly. This part will be discussed in Section 2.6.

2.4 Energy Flow and the Efficiency at Each Transfer

There are many energy transfer processes in our laser system. These processes are summarized and illustrated by the following figure.

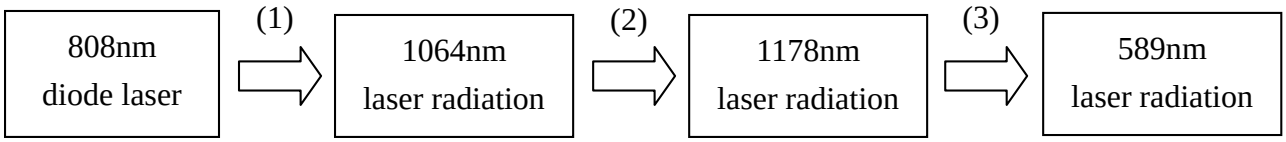

Figure 2.2 Illustration of energy transfer processes in our Raman laser

There are basically three important energy transfer steps, which are labeled as (1), (2), and (3) respectively. As for (1), the efficiency at this stage is determined by the spatial overlapping between the pump diode laser beam and the cavity TEM_{00} mode of 1064nm. The cavity mode is designed and determined by the whole cavity which consists of many optical components. The mode-matching lens set is used for adjusting the pump beam size and the diffraction angle in the laser gain medium, Nd:YVO_4, such that good coupling efficiency is achieved. Although the pump laser diffracts fast within a short distance, good coupling efficiency is obtained because of good absorption in Nd:YVO_4 within a short distance. As for (2), the efficiency depends on the spatial overlapping between the fundamental cavity modes of 1064nm and the Stokes wave. The cavity modes actually depend on the location of each crystal. On the other hand, thermal effects such as thermal lensing in the gain medium for the fundamental wave and the Raman crystal will affect the cavity mode, too. As a result, the cavity stability and the spatial overlapping between cavity modes are changed, and thus the laser performance is strongly dependent on thermal lensing. Furthermore, thermal lensing generally has different degrees of influence in variation with the pump power or the pulse repetition rate [37] when operated in pulsed scheme. For different kinds of crystals, the sensitivities to different pulse repetition rates are different. Therefore, it is really complex when considering both the thermal lensing

and the pulse repetition rate in optimizing the cavity mode overlapping. Additionally, since 1064nm and 1178nm are different wavelengths, their modes cannot be perfectly matched intrinsically. The cavity simulation of our Raman laser will be reported in Section 2.6. As for (3), the cavity modes are changed due to the insertion of SHG crystal. The efficiency is determined by factors mentioned in the end of Section 2.3.

2.5 Methods of Narrowing Down the Laser Bandwidth

2.5.1 Intracavity Etalon

In our experiment, we intend to try two ways for narrowing down the linewidth at 589nm. The first one is using an intracavity etalon. By carefully designed thickness and coatings of the etalon, the linewidth of the laser radiation can be limited and designed. For single longitudinal mode operation, the free spectral range (FSR) of the etalon should be larger than the gain bandwidth of the laser wavelength of interest, and the bandwidth of the single peak of transmittance provided by the etalon within the gain bandwidth should be less than the FSR of the cavity. Multi-mode operation is achieved if there are still few longitudinal modes that can pass the etalon with high transmittance. By inserting an etalon into the cavity, the linewidth is restricted during the process of stimulated emission, which is an amplification process for photons. Thus the linewidth of the output laser can be limited during the amplification process, giving rise to narrow-linewidth laser radiation.

In our Raman laser system, however, there are two wavelengths oscillating simultaneously in the shared cavity. On the other hand, the generated yellow light by the intracavity SHG will be emitted to two sides of the cavity. Therefore, it is difficult

to find a suitable etalon to restrict the radiation linewidth of both the fundamental wave and the Stokes wave or only restrict the Stokes wave, but without affecting the transmittance of the rest wavelengths at the same time. From our present available optics, we have proposed an idea to form an etalon coupler for use in our experiment. This part will be left to Section 3.2.1 for further discussions.

2.5.2 Grating Feedback at Grazing-Incidence

In 1972, Hänsch reported a nitrogen-laser-pumped dye laser using a diffraction grating in a Littrow mounting as well as an intracavity beam expander to tune the wavelength and narrow down the linewidth [38]. Afterwards, Shoshan et al. in 1976 [39], and Littman and Metcalf in 1978 [40], introduced independently a new design to narrow down the linewidth of a pulsed dye laser by using a grating. The grating is used at grazing incidence. That is, the laser beam incident on the grating has a large incident angle, such as larger than 85 degrees, typically. In this way, the full width of the grating can be utilized to achieve high angular dispersion. Small part of the beam was diffracted, and the large part was reflected by the grating along the path of zeroth-order diffraction. This zeroth order diffraction beam was used as the laser output. In Littman and Metcalf's design, they used a high reflector M to reflect the minus-first-order diffracted beam into the original path of incidence on M. Due to the high angular dispersion, the diffracted lights at different diffraction angles possess a range of angle even though the incident light is a laser. Therefore only part of the diffracted beam within a small wavelength range was chosen to be reflected into the original path. This reflected part would be incident on the grating again, diffracted by the grating, and propagate into the cavity as a seeding signal. This seeding signal with

a narrow linewidth would participate in the process of stimulated emission and the forming of light pulses, and thereby resulted in narrow-linewidth laser output. Furthermore, by rotating the high reflector M, the back-reflected beam would possess different wavelength range, and thereby the output laser wavelength can be fine-tuned. On another hand, the zeroth-order diffraction generated by the second incidence on the grating was lost.

The first main difference between Littman and Metcalf's design and that of Hänsch is that there are two incidences on the grating in Littman and Metcalf's design rather than just once in the other, and thus the linewidth of the reflected beam back into the cavity is narrower. The second main difference is the beam expander is unnecessary in the new design, leading to much simpler alignment. This kind of novel design was demonstrated successfully in their experiments. Additionally, it was demonstrated to be useful in an external-cavity diode laser in 1991 [41], and a grating-tuned, single longitudinal mode, diode-pumped Nd:YVO_4 laser in 1993 [42], and a periodically poled $LiNbO_3$ optical parametric oscillator in 1999 [43]. More recently, a single-longitudinal-mode, tunable dual-wavelength, CW Nd:YVO_4 laser was achieved in 2006 by using this method [44]. Therefore we are motivated to use a grating at grazing incidence to narrow down the linewidth of our Raman laser. Further discussions about the experimental setup are addressed in Section 3.2.2.

2.6 Thermal Lensing in Nd:YVO_4 and $CaWO_4$ and Cavity Simulation

Based on the concepts introduced in previous sections, it is important to realize the physical mechanisms of thermal problems and try to model the cavity dynamics. In this section, origins of thermal lensing referred to [18] will be briefly addressed and simulation of our Raman laser is presented.

In our experiment, thermal problems come from the excess heat generated during the pumping process and the inelastic nature of Raman scattering as mentioned in Chapter 1. The generated heat will diffuse from the hotter area to the cooler area, resulting in a temperature variation. The temperature variation depends on the material properties and the geometry of the crystal and the laser system. For example, the heat conductivity of the crystal may not be the same in all directions. The pumping scheme such as an end-pumped system or side-pumped system is also a factor, because different schemes produce different kinds of heat source inside the crystal, and thereby the ways of heat diffusion will be different. The cooling system is also a factor, because different kinds of system provide different kinds of way for heat dissipation. In our system, Nd:YVO_4 was placed in a water-cooled copper block which surrounded four sides of the crystal except for the two end-faces. The two end-faces are directly touched with air, and one side is pumped by the diode laser. Apparently, the diffusion of heat will be complicated and asymmetric. In fact, there are many other effects accompanying with heat diffusion. For instance, thermal stress results from the expansion of the hotter area that is constrained by the cooler area. Mechanical stress is raised and the crystal structure was deformed, resulting in changes of refractive index. Also, temperature variation gives rise to temperature gradient in variation with space coordinates. The temperature gradient will deform the crystal structure such that different areas possess different degrees of deformation, making refractive index of the material change from the hotter side to the cooler side. Thermal lensing is a thermal effect in the sense that the refractive index of the crystal is modified by heat diffusion, and the variation of refractive index makes the crystal like a positive or negative lens, depending on material properties. Since different pump powers give rise to different amount of excess heat, and thus results in different degrees of thermal lensing effect. Thermal lensing effect will affect the cavity mode

and system stability substantially. Some phenomena such as aberrations due to thermal lens may further degrade the laser system. On another hand, it was reported that the thermal loading depends on the pulse repetition rate in a diode-end-pumped Q-switched laser, and thus the cavity stability and cavity mode are affected by the pulse repetition rate [37]. This part will be discussed in Chapter 3 to explain our experimental results. Actually thermal effects are really complex but well-studied in the literature.

In the following, without considering the pulse repetition rate, I try to calculate the beam radius on the input mirror and output coupler at different thermal focal lengths first, and then estimate the thermal focal length of the crystal at different pump powers. In this way we can know the beam radius at different pump powers. The simulation results can be a reference for our experiment. Note that the thermal lensing generally has long thermal focal length in $CaWO_4$. As shown in Table 2.1, the thermal focal length in $CaWO_4$ is generally well above 1m, and thus we will only consider the thermal lensing effect in Nd:YVO_4 but not in $CaWO_4$ for simplicity. Refer to [45] [46]; see Figure 2.3 below for a cavity containing a thin lens.

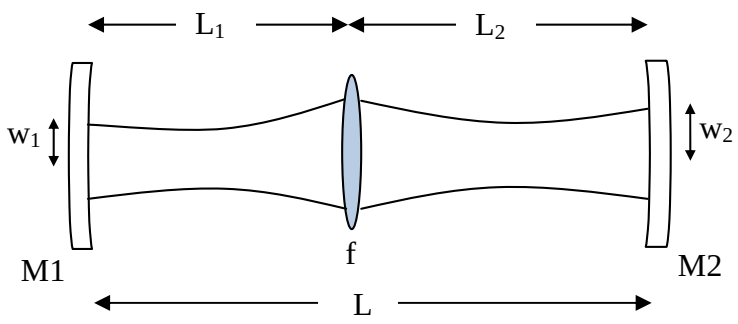

Figure 2.3 A cavity containing a thin lens

where w_1 and w_2 are beam radii at mirror M1 and M2, respectively; L_1 is the distance between M1 the thin lens; L_2 is the distance between the thin lens and M2; f is the

focal length of the thin lens. Then we have:

$$L = L_1 + L_2$$

$$g_1 \equiv 1 - \frac{L_2}{f} - \frac{L_0}{R_1} \quad ; \quad g_2 \equiv 1 - \frac{L_1}{f} - \frac{L_0}{R_2}$$

$$L_0 \equiv L_1 + L_2 - \frac{L_1 L_2}{f}$$

$$w_1^2 = \frac{l\,L}{p}\left[\frac{g_2}{g_1(1-g_1 g_2)}\right]^{\frac{1}{2}} \quad ; \quad w_2^2 = \frac{l\,L}{p}\left[\frac{g_1}{g_2(1-g_1 g_2)}\right]^{\frac{1}{2}} \qquad (11)$$

The above equations for beam radii can be obtained by solving the equation in which the complex q parameter remains the same after applying a round-trip ABCD matrix of the cavity to it. The thin lens in Figure 2.3 can be modeled as the thermal focal length of the thermal lens. Therefore we can find the relation between the beam radius on the mirror and the thermal focal length.

Let us refer to [47] for further investigation. When inserting a thick lens of refractive index n into the cavity, the cavity can be modeled as an equivalent thin lens model as shown in Figure 2.3. The modifications for the transformation are as follows. Refer to Figure 2.4,

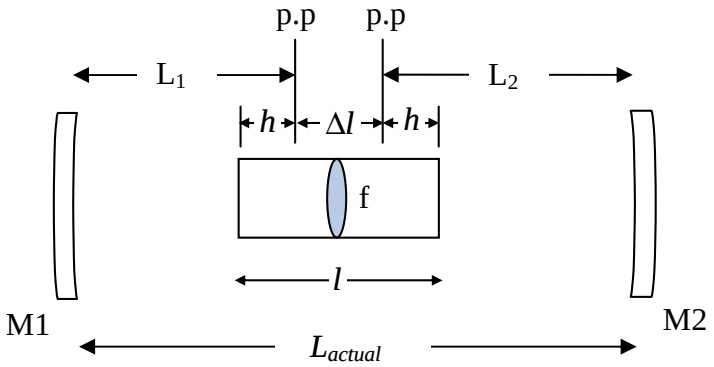

Figure 2.4 A cavity containing a thick lens

where $h = \frac{l}{2n}$; $\Delta l = l\left(1 - \frac{1}{n}\right)$; l is the thickness of the lens; L_1 is the distance between M1 and the principal plane (p.p.) of the thick lens; L_2 is the distance between

M2 and the p.p. of the thick lens. The equivalent thin lens model is just that shown in Figure 2.3 with the same L_1 and L_2 in Figure 2.4. Note that the location of the p.p. does not change at different pump powers. Therefore, if we insert a crystal of refractive index n into the cavity, the effective cavity length in the corresponding thin lens model is L_1+L_2, which is shorten by $\Delta l = l\left(1-\frac{1}{n}\right)$ from the actual cavity length, $L_{actual} = L_1 + L_2 + l\left(1-\frac{1}{n}\right)$. This is because that the refraction in the material changes the cavity mode. In our experiment, the crystals in the cavity include:

Materials	Refractive Index	Shorted length $\Delta l = l\left(1-\frac{1}{n}\right)$
Nd:YVO_4 ($3x3x9mm^3$)	$n_o = n_a = n_b = 1.9573$ $n_e = n_c = 2.1652$@1064nm	Δl_1 ~4.40mm
$CaWO_4$ ($9x9x40mm^3$)	n~1.9 @1064nm	Δl_2 ~18.96mm
LBO ($3x3x25mm^3$)	n_x=1.5656@1064nm n_y=1.5905@1064nm n_z=1.6055@1064nm	Δl_3 ~9.03mm
Q-switch crystal (crystal quartz, length=25mm)	n_o=1.534@1064nm n_e=1.543@1064nm	Δl_4 ~8.75mm

Table 2.4 Refractive indices of crystals inside the cavity and the corresponding shortened lengths in our Raman laser

Assume that the thin lens in Nd:YVO_4 is at the center of the crystal. Thus the equivalent L_1 in our experiment is L_1=8mm-Δl_1/2(=2.2mm)=5.8mm, where 8mm is the measured actual length of L_1; the equivalent L_2 when considering all crystals in Table 2.4 is (128mm is also a measured actual length of L_2):

L_2=128mm- Δl_1 /2(=2.2mm)- Δl_2 (=8.96mm)- Δl_4 (=8.75mm)- Δl_3 (=9.03mm)~89.7mm

If in the experiment without adding LBO, L_2~98.09mm

Note that $L_{2,\,actual}$ is fixed at 128mm in the experiment.

For the cavity mode of 1064nm, from (11) and Table 3.1 (concave-planar) we get:

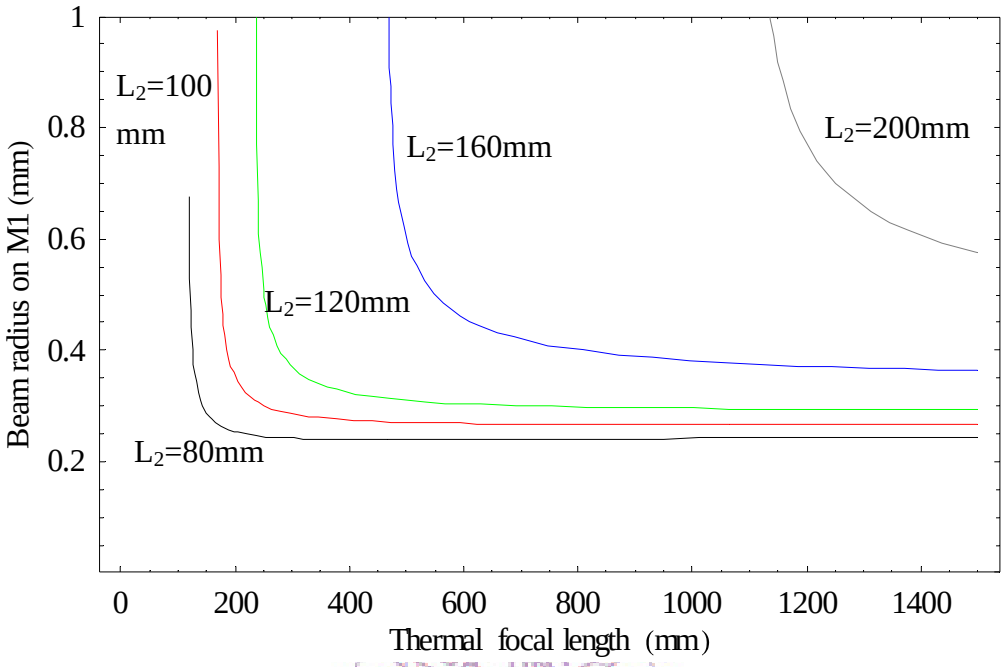

Figure 2.5 Beam radius on M1 with respect to the thermal focal length at different L_2

Figure 2.5 shows the beam radius on M1 in variation with different thermal focal lengths at different equivalent L_2 when considering the adopted mirror in our experiment. Different L_2 represent different cavity lengths since equivalent L_1 is fixed in the experiment. In our case, the equivalent L_2 including all crystals is around 90mm, which corresponds to a curve between the black and red curves in Figure 2.5. When the pump power increases, the thermal focal length decreases. At f~150mm, we see that L_2=100mm intends to become unstable. If we further increase the pump power, cavity with L_2=100mm becomes unstable and cavity with L_2=100mm starts to become

unstable.

In conclusion, f~150mm is probably the limit in our cavity design. Furthermore, because the mode size becomes larger when cavity length decreases at the same thermal focal length, it is better to keep the cavity short to avoid instability at high-power state, and in the meanwhile keep the mode size small enough to have high intracavity intensity for nonlinear wavelength conversion.

For the beam radius on M2, we get Figure 2.6 similarly.

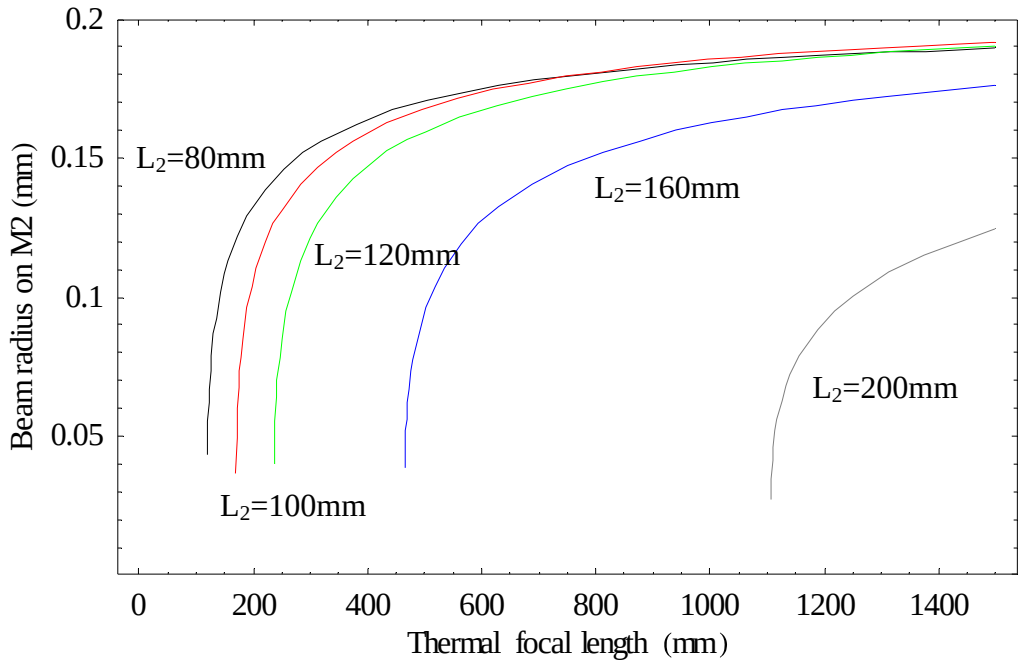

Figure 2.6 Beam radius on M1 with respect to the thermal focal length at different L_2

From the pump efficiency point of view, we see that when the pump power increases, the mode size on M1 increases while on M2 decreases. The mode size should be well-matched with the pump spot size in Nd:YVO_4, so that the coupling efficiency could be good. If the pump spot size is larger than the fundamental mode size, other higher-order transverse modes may be excited. The coupling efficiency from the pump laser to the fundamental mode would become lower.

The condition of a stable cavity is: $0 < g_1 g_2 < 1$. Put the characteristic values in

our experiment into the inequality, we get $f > 142.53mm$ for L_2=89.7mm

$f > 163.97mm$ for L_2=98.09mm

Refer to [48]. In an end-pumped system, we have the following formula by considering only the temperature dependent part of thermal lensing, and assume that there is only radial heat flow in the crystal which contacts with the cooling system at fixed temperature:

$$f = \frac{p K w_p^2}{P_h \frac{dn}{dT}} \left(\frac{1}{1-\exp(-a_o l)} \right) \tag{12}$$

where f is the effective thermal focal length, K is the thermal conductivity of the material, w_p is the $1/e^2$ Gaussian radius of the pump laser beam, P_h is the fraction of the pump power that gives rise to heating, dn/dT is the change of the refractive index with temperature, a_o is the absorption coefficient, l is the crystal length.

Because I am not sure about the real parameters of our Nd:YVO_4 so far, I assume the K of Nd:YVO_4 is 0.052W/cm K; w_p ~400 mm ,which is a typical value; dn/dT~4.7×10^{-6}/K; a_o ~$31.4cm^{-1}$; l=9mm; for P_h, usually 30% of the pump power results in heat. The above characteristic values are referred to some other Nd:YVO_4 crystal temporarily. Use (12), some calculated thermal focal lengths are shown below:

Pump power = 5W, f = 370.75mm;

10W$\Rightarrow$ f = 185.38mm;

13W$\Rightarrow$ f = 142.60mm;

15W$\Rightarrow$ f = 123.58mm;

18W$\Rightarrow$ f = 102.99mm;

20W$\Rightarrow$ f = 92.69mm;

25W$\Rightarrow$ f = 74.15mm.

The following figure shows the variation:

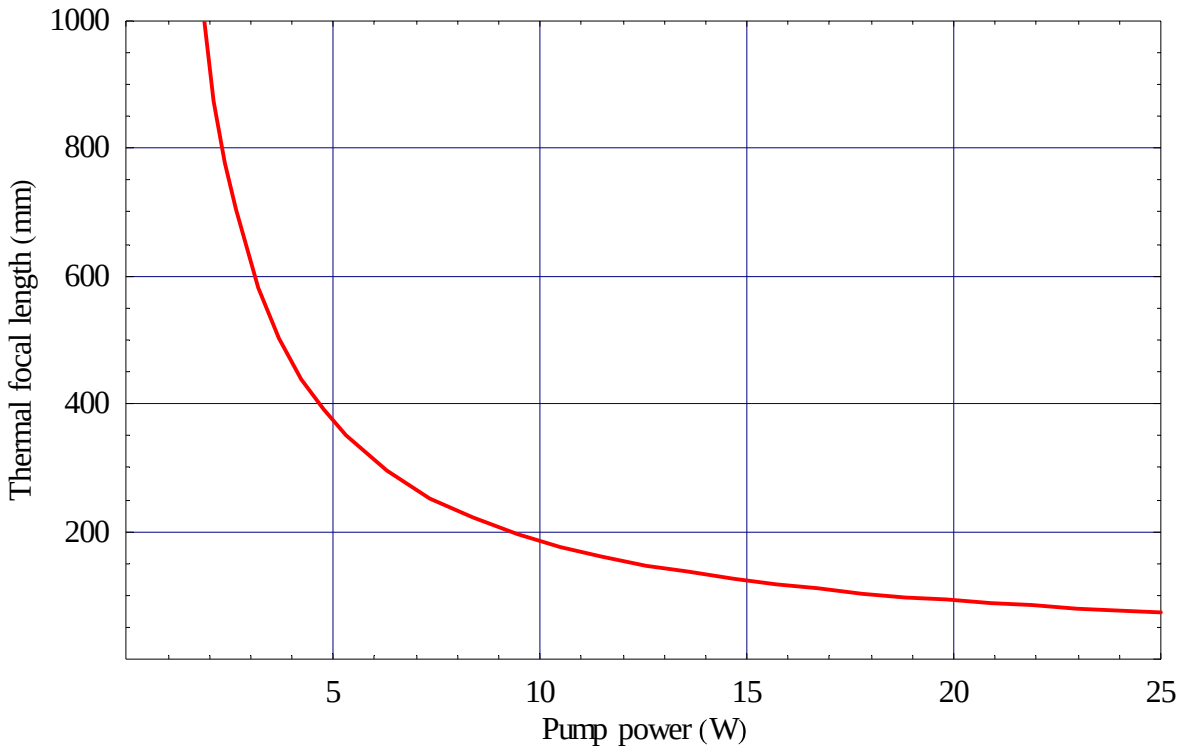

Figure 2.7 Thermal focal length versus the pump power in Nd:YVO_4

Note that Figure 2.7 is just for reference when doing the experiment, since the characteristic values of Nd:YVO_4 is not real ones and the model for the thermal focal length is a simplified version, in which many other thermal problems have not been considered.

In summary, the cavity looks highly dynamic due to many thermal effects which vary with the pump power and pulse repetition rate. Different pump powers or pulse repetition rates correspond to different cavity modes. Thus one has to optimize the system in each case for the best performance in that case. We can refer to the simplified simulation results as reminders when doing the experiment. They are also helpful in calculation of the mode size. In fact, the final optimization is achieved empirically [21], especially in a laser system containing many optical elements.

Chapter 3 Experimental Results and Discussions

3.1 Introduction

In order to generate artificial guide stars for the application in adaptive optics, there are many requirements for the sodium-yellow laser as mentioned in Chapter 1. Based on the work of James T. Murray et al, we therefore intended to improve two main factors, that is, the average power and linewidth of the yellow laser. As for the average power, we would like to do intracavity SHG to improve the SHG efficiency in [15]. On the other hand, we have tried to narrow down the linewidth by using an etalon coupler or through a grating feedback. In summary, we propose two possible configurations for generating higher average output power and narrow linewidth at 589nm in this dissertation.

In this chapter, we will report our experimental setups, and the performance of the laser systems based on the considerations mentioned above. Detailed parameters of the components and setups are reported in Section 3.2. Results will be reported, discussed and analyzed in Section 3.5.

3.2 Configurations of the Raman Laser

3.2.1 Raman Laser with an Etalon Coupler

In this section, we will report the results based on the following configuration, as shown in Figure 3.1, and then discuss the feasibility of this kind of setup.

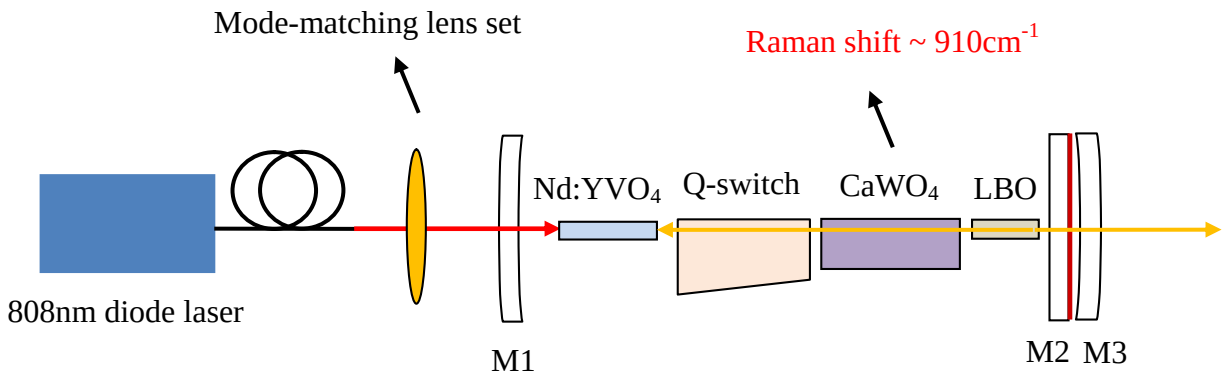

Figure 3.1 The configuration of the Raman laser with an etalon coupler.

First, let us look into the setup shown above without M3. Conceptually speaking, the coatings on M1 and M2 are preferred to be high reflective (HR) at 1064nm so as to make the cavity confine the power of 1064nm well, such that the high intracavity power of 1064nm can be attained, having good interaction between 1064nm laser and $CaWO_4$. Here we hope HR could be at least R>99.5%; R>99.9% is even better. As for the Stokes wavelength at 1178nm, M1 is also preferred to be HR at 1178nm, while the coating on M2 depends on the following considerations:

1. If we want to get as more average output power at 589nm as possible without caring about the laser linewidth, then M2 is preferred to be high reflective at 1178nm as well. That is, the cavity also confines 1178nm well so that we can utilize the high intracavity power of 1178nm to do intracavity SHG. We expect higher SHG efficiency can be achieved in intracavity SHG rather than extracavity SHG as mentioned in Chapter 2. In summary, M1 and M2 form a high-reflective shared cavity for both 1064nm and 1178nm waves, giving rise to good interactions between 1064nm laser and the Raman crystal, and between 1178nm laser and LBO crystal. The efficiency at each energy transfer process thus could

be raised so that high average output power at 589nm could be obtained.

2. If we want to take both the average output power and the narrow linewidth into account, then there are two ways that we can try to narrow down the linewidth while getting higher power than that of the extracavity-SHG configuration; it is possible if we do intracavity SHG as well as adopt the following methods: The first one is to use an etalon coupler, so that the laser linewidth can be limited and designed during the growing-up process of laser generation. The other one is to use a grating feedback such that the feedback signal can participate in the stimulated emission process of the Raman signal, producing narrower linewidth of the Raman signal. The feedback signal is acting like a seeding as mentioned in Chapter 2. We discuss in the etalon coupler first and leave the grating feedback to Section 3.2.2.

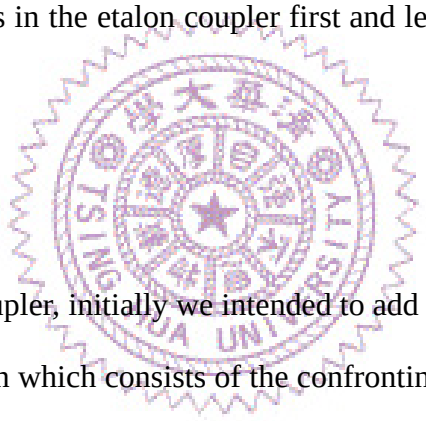

As for the etalon coupler, initially we intended to add another mirror M3 together with M2 to form an etalon which consists of the confronting faces of M2 and M3, and the air gap between them. As shown in Picture 3.1, the red line of the M2 indicates its surface with HR coating, which will be characterized in Table 3.1 below. In order to get narrow-linewidth output, actually we can design the coatings at 1064nm and 1178nm separately on M2 and M3 as well as the thickness of the air gap. In the experiment, we can tune the gap length to have high transmittance at the desirable wavelength. But when we considered M2 and M3 as a whole, that is, an effective etalon, we found that in fact this etalon behaved as the output coupler equivalently. Therefore the function of this “etalon coupler” seems weird in the sense that when we design the central wavelength and the linewidth for the output and let it go out of the etalon with high transmittance, it actually affects the gain spectrum of the cavity since

the etalon also plays the role as the output coupler. That is, we pick up the desired central wavelength, making it go through the etalon with high transmittance. But at the same time great loss is also caused at that wavelength such that the cavity mode of that wavelength component cannot oscillate in the cavity if the total gain is less than the loss. However, if the transmittance for the desired wavelength is not so high, the gain at that wavelength may be still larger than the loss, so that oscillation is still obtained, and the laser is emitted through the etalon.

Discussions above are for the desired central wavelength of the Stokes wave. The assumption is that the corresponding central wavelength of the fundamental wave still has high intracavity power in the cavity with the etalon as the output coupler. This may be possible because in the real experiment we tuned the gap length to make the etalon coupler have high transmittance at the Stokes wavelength. The transmittance at the fundamental wavelength may not be high since the wavelength is different from the Stokes wavelength.

Conclusion: so far we have discussed only the effect on the desired central Stokes wavelength. If further considering the gain bandwidth and the loss of the Raman signal together with the selective spectrum of the etalon, the original gain spectrum of the cavity actually becomes complex. It is hard to predict the output spectrum unless careful calculations are done. From the discussions above, we find that if we want to adjust one parameter to improve the corresponding performance, another parameter usually is changed accordingly and some undesired effect is caused on another performance, and vice versa. This is because M2 together with M3 act as the output coupler as well as an etalon. This dual property makes us unable to fine tune each parameter separately. Therefore the optimization process becomes very difficult. The feasibility seems almost impossible unless very careful considerations and calculations are done for a specific design. However, I am not sure if it can be

done in real design. Nevertheless, I still did the experiment even with uncertainty by using available mirrors to see what would happen. The results will be reported in Section 3.5.1.

The following picture is the real experimental setup:

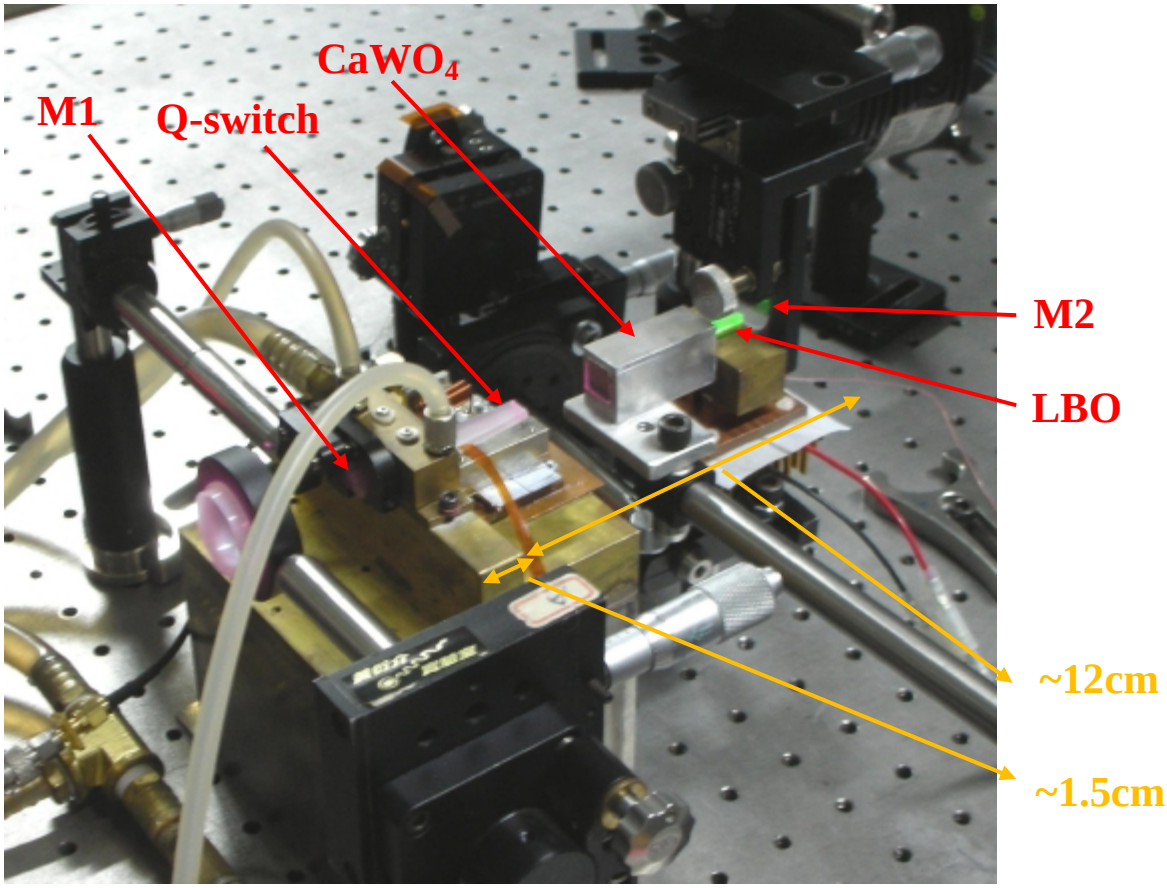

Picture 3.1 The picture of the real experimental setup.

Refer to Picture 3.1, the actual cavity length is around 13.5cm. The measured values have been analyzed by simulation in Section 2.6. The look of the mirror mount of M2 in the picture is for setting up M3 afterwards, since the air gap is around millimeters. The detailed parameters of mirrors are shown below. The given reflectance or transmittance are at the angle of incidence (AOI) of zero degrees.

HT: High Transmittance HR: High Reflectance PR: Partial Reflectance

M1	Concave mirror, radius of curvature (ROC) = 250mm Coating: HT@808nm R<5% HR@1064nm R>99.94% HT@589nm T~98.5% HR@1178nm R>99.75%
M2	Flat mirror Coating: HT@808nm R<5% HR@1064nm R>99.94% HT@589nm T>90% HR@1178nm R>96%
M3	Concave mirror, radius of curvature (ROC) =100mm Coating: HR@1064nm R: 98~99% PR@1178nm R~52%
M4	Flat mirror ; Coating: HR@1064nm&1178nm R> 99.8~99.9% (AOI=0) HR@1064nm&1178nm R> 99%(AOI=45 degrees)
M6	Flat mirror Coating: HR@1064nm&1178nm R> 99.9%

Table 3.1 Detailed parameters of mirrors

In the experimental setup, we used a fiber-coupled 808nm diode laser with maximum power up to 20W to pump a Nd:YVO_4 crystal, which was wrapped with the indium foil and placed in a water-cooled copper block as shown in Picture 3.1. The water was kept at room temperature. This water tank was used for dissipating the heat generated in the crystal because severe thermal loading will degrade the performance of the laser system greatly. In our experiment, we used a 3x3x9mm^3 a-cut Nd^{3+}:YVO_4 with doping concentration of 0.25-at.% and AR coating at 1064nm. Additionally, a

3x3x25mm^3 LBO with AR coating on 1064, 1178, and 589nm was placed on a thermal-electric (TE) cooler, which could raise or lower the temperature to achieve the NCPM temperature for SHG of 1178nm. Both the water-cooled system and the TE cooler will be introduced briefly in Section 3.3. Note that $CaWO_4$ with AR coating at 1064 and 1178nm was just placed in a holder without further cooling. The heat generated due to the inelastic nature of Raman scattering is just conducted to the holder and the metal mount. For Raman crystals having significant thermal lensing effect or severe thermal loading, a cooling system is absolutely necessary to avoid degradation in laser performance resulted from thermal problems. The mode-matching lens set with an 80% coupling efficiency from the diode laser output to the end of the lens set consisted of a ball lens and a positive lens with focal length of 25mm. It was responsible for the purpose of coupling energy from the diode laser to the cavity modes effectively, and will be investigated in Section 3.4. Some parameters of the crystals used in the experiment are already shown in Table 2.1, 2.2, 2.3, and 2.4.

The laser was a concave-planar resonator design. In this arrangement, initially we wanted to put a grating at grazing incidence near M2, and used the zeroth-order diffraction beam to do extracavity SHG as shown in Figure 3.2. However, we found that the insertion of the grating resulted in large loss, making the average power of the zeroth-order beam less than that of the direct output from M2 significantly. On the other hand, the coating on M2 does not have an optimized value to maximize the output power of 1178nm due to the unavailability in optics. Therefore, we gave up this design, turned to a modified one in Section 3.2.2 and hope that it is better.

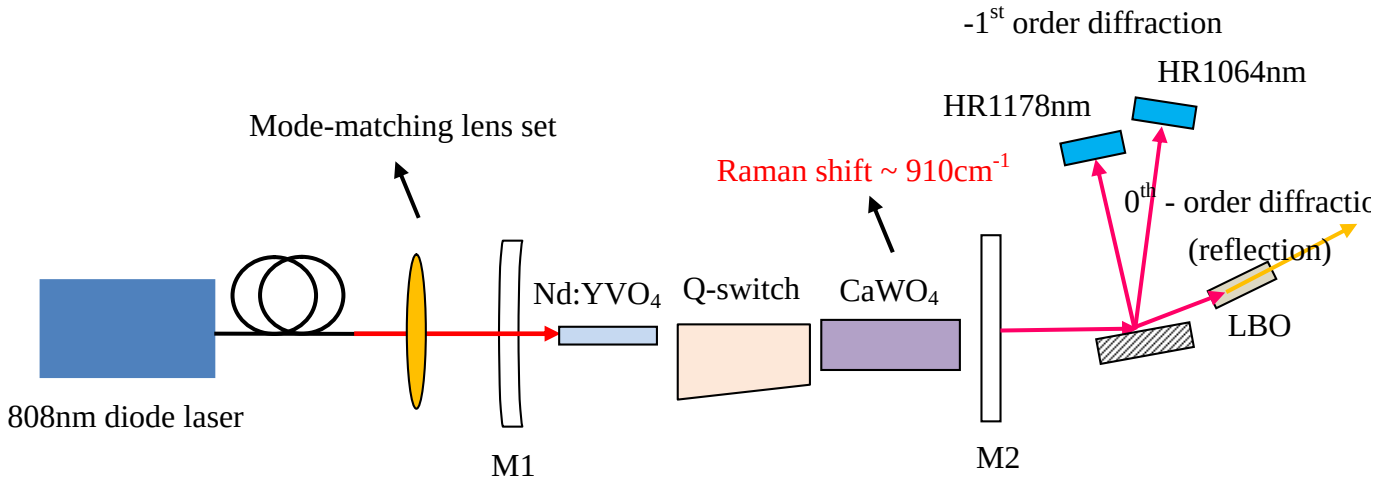

Figure 3.2 The configuration of the Raman laser with a grating feedback and extracavity SHG

Before adding M3 and LBO into the laser system in Figure 3.1, we intended to investigate the properties of the Raman laser without M3. In this way, I wanted to get some feeling about the output characteristics and gain some real experiences in this linear cavity, such that I can handle the folded cavity configuration in Section 3.2.2. The results will be shown in Section 3.5.1.

3.2.2 Raman Laser with a Grating Feedback

Based on Figure 3.2, a possible way to avoid the large loss due to the insertion of the grating is to utilize the high intracavity power rather than the direct output power, because the output coupler M2 actually does not have an optimized coating to maximize the output power at 1178nm, meaning that the yellow power obtained after extracavity SHG is limited by this constrain. On another hand, due to the little loss at 1178nm of M2, some Stokes wave can still be coupled out to be incident on the grating, so that we can feedback the refracted light to narrow down the linewidth and just ignore the zeroth-order light. In this way, we do not have to worry about the available output power from M2, because we can utilize the high intracavity

power and hopefully still get narrower linewidth.

However, the possible difficulties may be a more complex cavity design due to the insertion of LBO into the cavity, and the uncertainty in the effectiveness of the grating feedback. The cavity design has been discussed in Chapter 2. As for the grating feedback, a compromise appears. If the loss at 1178nm of M2 is very little, we can have higher intracavity power of the Stokes wave but little for coupling out. The insignificant Stokes output will pass through the grating twice and then be reflected back to M2, which has little transmittance for it, so the feedback signal becomes much weaker. Thus we are not sure whether the feedback signal is strong enough to narrow down the linewidth effectively. On the other hand, if the loss at 1178nm of M2 is a little bit larger, then the intracavity power will drop but the power for coupling out will increase. Therefore after reflection to the cavity, the feedback signal becomes stronger. Unless careful calculation has been down, we cannot know the best policy. Another consideration is the interaction between the feedback pulsed signal and the original Stokes pulse. Actually due to time for passing the grating and reflected back, the feedback signal would participate in the later process of growth of the Stokes pulse. Unlike the CW case, pulsed operation thus raises some limitations in narrowing down the linewidth. Therefore the number of passes of a Stokes pulse in the cavity seems to be an important factor, because it determines the interaction time between the original Stokes pulse and the feedback signal.

Notice that the above discussion is about the Stokes wave at 1178nm. As for the fundamental wave, in order to have good interaction with the Raman crystal, the reflectance at 1064nm of M2 is preferred to be very high. But in this way it means that the feedback for 1064nm may have insignificant effect. However, it is probably preferred to confine the fundamental wave well in the cavity to have good wavelength conversion rather than couple out some fundamental wave for feedback purpose,

because a little bit 1064nm coupled out may increase the Raman threshold remarkably due to the exponential Raman gain which has the intensity of the fundamental wave as the exponent. Thus I will consider the feedback setup for 1178nm, and do the experiment without feedback for 1064nm first.

Due to many uncertainties, I would like to do this experiment without much calculation on the grating feedback first, and hope that experiences and experimental results may give me a direction to optimize the system.

It is natural to have the following arrangement based on the above discussion.

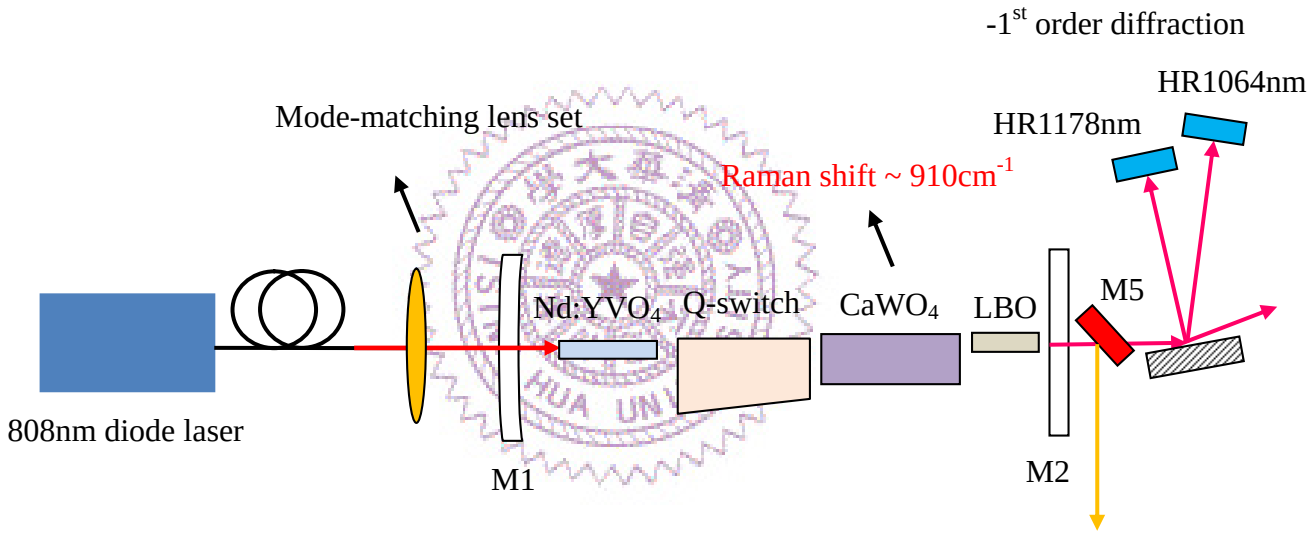

Figure 3.3 A possible configuration of the Raman laser with a grating feedback

Note that a special mirror M5 is needed to have high transmittance at 1064 and 1178nm but high reflectance at 589nm to extract the generated yellow light from the co-propagating laser beam. Because of the unavailability of M5, we will not adopt this configuration. We resort to a folded cavity shown in Figure 3.4.

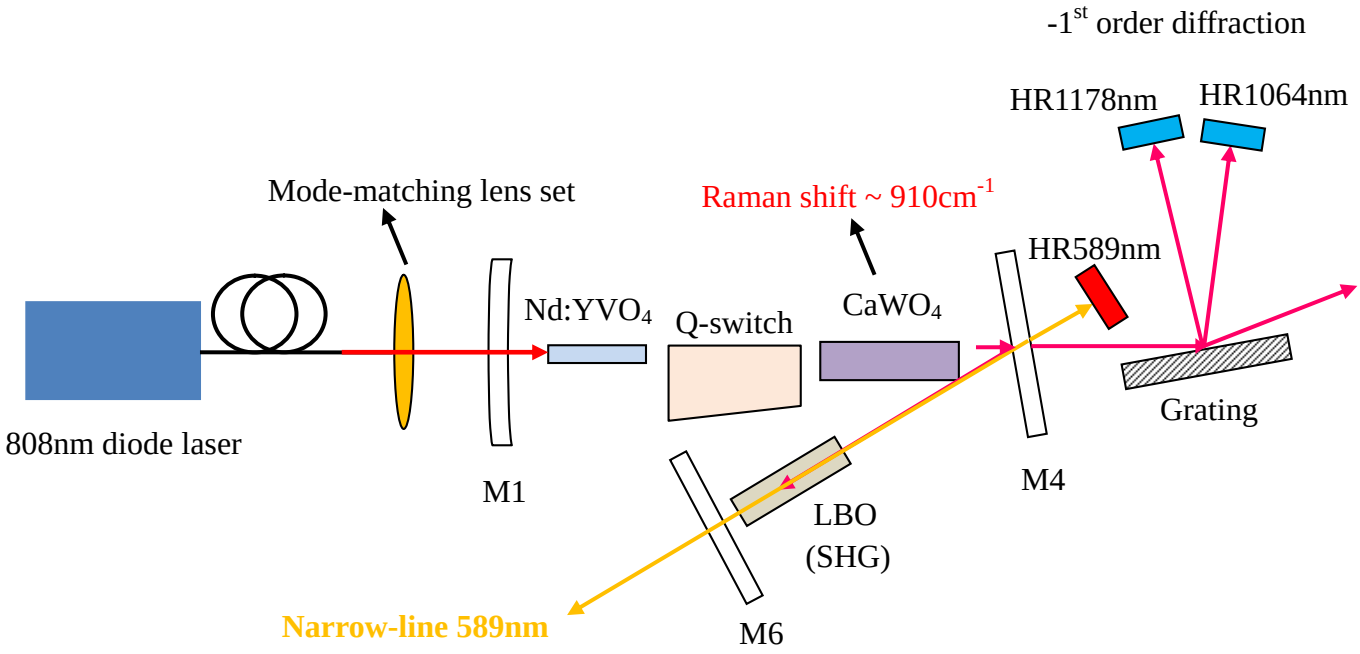

Figure 3.3 The configuration of a folded Raman laser with a grating feedback

In Figure 3.3, basically the folded cavity formed by M1, M4, and M6 is preferred to have high reflectance at both 1064 and 1178nm except that M4 has high reflectance at 1064nm but little loss at 1178nm. The specifications of coatings on mirrors are shown in Table 3.1 in the Section 3.2.1. Note that M4 is a commercial product specified at AOI=45 degrees. The values at AOI=0 are measured in the experiment. We would like to rotate M4 to change the reflectance such that some 1178nm wave can be coupled out for the grating feedback. We first measured the transmittance versus wavelength at different AOI by using a spectrophotometer, and then referred to the measured values when doing the experiment. The grating we used was a gold-coated grating with 1200 grooves/mm. Notice that the polarization of the laser has to be perpendicular to the grooves of the grating so as to get the maximum diffraction efficiency [42].

In the experiment, the yellow light will be generated in the forward and backward directions, and therefore M4 is preferred to have high transmittance at 589nm so that we can collect the yellow light by using a HR589nm mirror as shown in the figure. We have to fine tune the location of HR589nm mirror so as to make the

reflected yellow light have constructive interference with the forward-propagation light. However, since in reality there is partial reflectance at 589nm of M4, the backward-propagation yellow light will pass through the intracavity optical elements and may cause some thermally induced effects.

3.3 Cooling and Temperature-Controllable Systems

3.3.1 Water Tank Cooling System

The water tank cooling system in our Raman laser was made by a group member for use in a diode-end-pumped solid-state laser [49]. It has many pipes for water to circulate such that the excess heat generated in the Nd:YVO_4 can be dissipated and the thermal loading can be alleviated. The mount for the crystal is made of copper for good heat conduction. Water pipes are connected to a motor put inside a barrel containing water which is kept at the room temperature. Note that the water vapor will increase the moisture. Some crystals such as LBO will absorb moisture from the air and melt. Thus the humidity has to be controlled by dehumidifier definitely.

3.3.2 Thermal Electric Cooler with a Temperature Controller

In order to achieve the NCPM temperature for SHG of 1178nm in LBO, I have designed a temperature-controllable system to tune the temperature. The system includes a crystal mount made of copper, a TE cooling chip, a heat sink, and a temperature controller. The TE cooling chip is sandwiched in between the copper mount and the heat sink. We used heat sink compound to be the connection at the interface. Plastic screws were used to fix the copper mount on the heat sink to avoid

the heat conduction from the hot side to the cold size of the TE chip. A sensor was implemented into the copper mount to provide feedback information to the temperature controller. The whole system can be an oven to raise the temperature or be a cooler to lower down the temperature, depending on the current direction we adopt. Reverse the direction of the current will change the function of the system. The system has no fan to avoid blowing dust onto the crystal surface; it relies on air cooling and can be operated from 0 to 60 degree C.

3.4 Investigation of the Mode-Matching Lens

An end-pumped solid-state laser system usually uses the conventional mode-matching lens set to achieve the best overlapping between the pump laser beam and the fundamental transverse mode of the laser cavity. The lens set consists of two separate lenses, one for the purpose of collimation of the pump laser beam, and the other for refocusing the collimated pump beam. However, in our experiment, we used a ball lens together with a single focusing lens with focal length 25mm to couple the energy from the pump laser at 808nm to the fundamental transverse mode of 1064nm. Thus, we have to investigate whether this lens set works well by setting up a diode-end-pumped Nd:YVO_4 laser, and compare the average output power with others' results in the same kind of laser system, in which conventional lens set is used. In our experiment, the cavity length was around 6.2cm. The following Table 3.2 shows the relation between the diode current (Ampere) and the diode pump power (Watt) from the diode laser. The curve of CW average output power (W) versus diode current (A) is shown in Figure 3.4. We have found that lasing was achieved when the pump current was 7A. At 7A, the output power at 1064nm was 0.14W; at the maximum pump current, 34A, the output power was 9.36W. In comparison with others' results, it is sure that the lens set in our system works well so that there is good

mode matching between pump laser beam and the fundamental cavity mode.

4A	5A	6A	7A	8A	9A	10A	11A	12A
8mW	14mW	0.24W	1.04W	1.85W	2.73W	3.63W	4.53W	5.41W
13A	14A	15A	16A	17A	18A	19A	20A	21A
6.28W	7.13W	8.01W	8.92W	9.76W	10.62W	11.39W	12.23W	13.09W
22A	23A	24A	25A	26A	27A	28A	29A	30A
13.94W	14.93W	15.81W	16.51W	17.32W	18.07W	18.55W	19.20W	19.92W

Table 3.2 This table shows the relation between diode current (A) and diode pump power (W) from the diode laser. The power below each operated current of the diode laser is the diode pump power for the laser system.

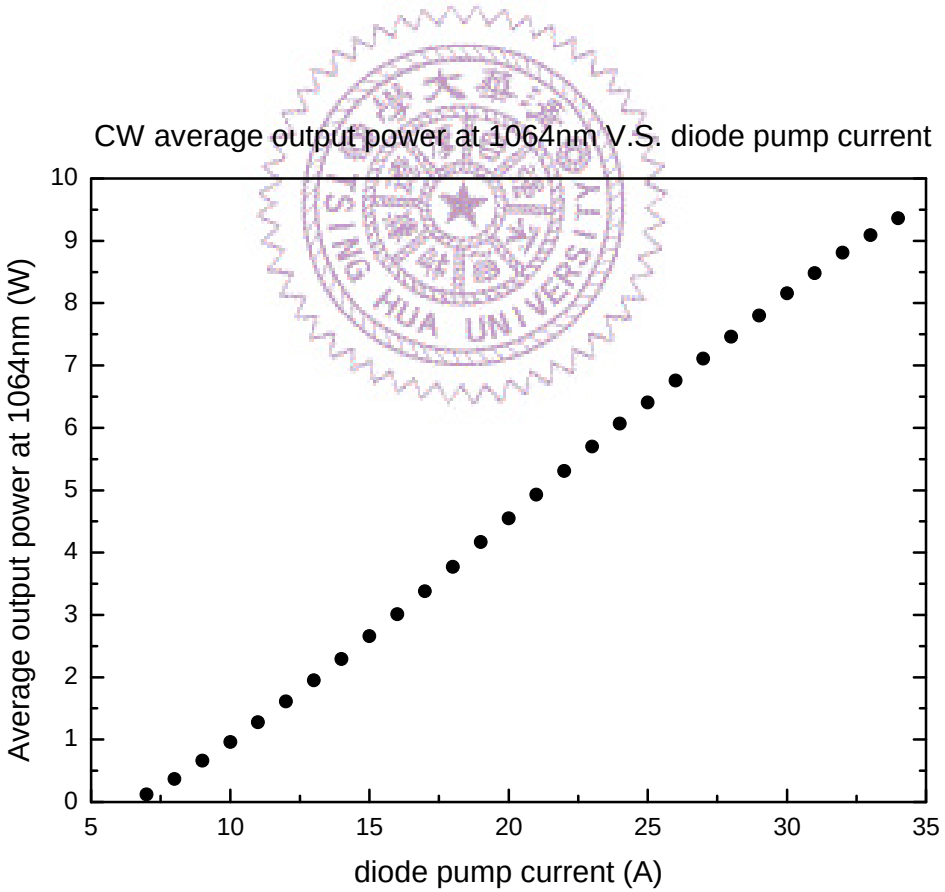

Figure 3.4 This figure shows the relation between CW average output power at 1064nm and diode pump current. Lasing was achieved when the pump current was 7A. At 7A, the output power at 1064nm was 0.14W; at the maximum pump current, 34A, the output power was 9.36W.

3.5 Experimental Results

3.5.1 Raman Laser with an Etalon Coupler

We investigated the system shown in Figure 3.1 without LBO and M3 first, and then measured the spectrum property after adding M3.

In the experiment, we have found that the $CaWO_4$ crystal seemed to grow inhomogeneously. Actually it is not a commercial product and the real parameters are not specified. We have polished the crystal and sent it for AR coating at 1064 and 1178nm. We found that only a small part of the crystal would provide a high Raman gain coefficient. See Picture 3.2 (a) below. The area with light color was found to be the active region to provide a high Raman gain coefficient; the area with dark color provided an insignificant Raman gain coefficient, and thus it was hard to achieve the Stokes generation in this region.

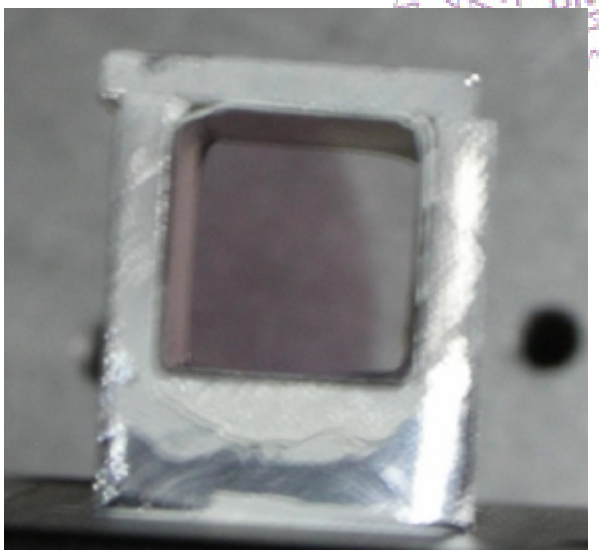

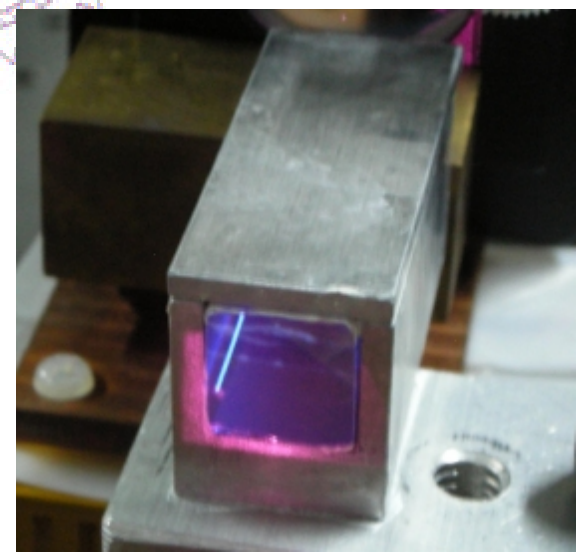

Picture 3.2 (a) The transverse view of $CaWO_4$ **(b)** The transverse view of $CaWO_4$ when lasing at 1178nm

Picture 3.2 (b) shows the transverse view of $CaWO_4$ when lasing was achieved at 1178nm. Therefore, when doing the experiment, we aligned the optical axis to pass through the area with light color. In the folded cavity, in fact, this situation increases the difficulty in alignment for us to keep the cavity length short, because a large part of the crystal is unavailable and occupies the space.

The following Figure 3.5 is a typical output spectrum observed by an optical spectrum analyzer (OSA).

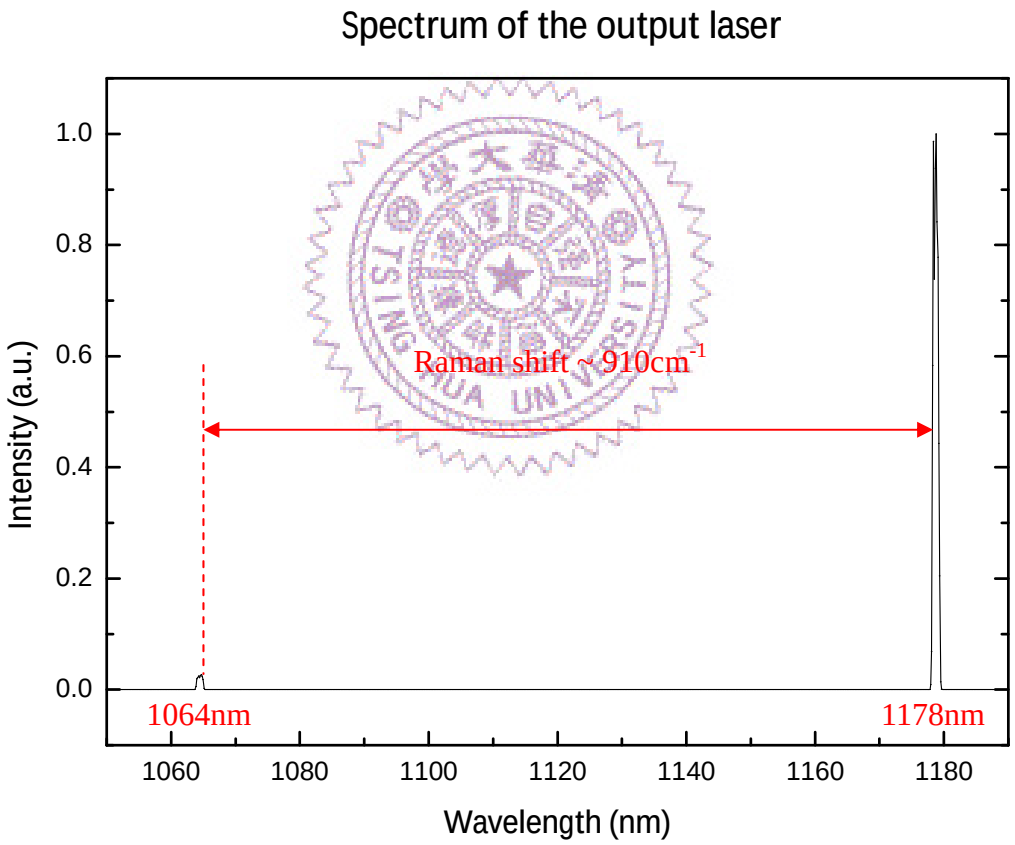

Figure 3.5 A typical output spectrum observed by an optical spectrum analyzer (OSA) The vertical scale is linear.

From the spectrum, the corresponding Raman shift, 910cm^{-1}, is consistent with the reported values. The following output spectrum in Figure 3.6 shows the generation of the first Stokes wave at 1103.5nm corresponding to the peak of another Raman shift ~333cm^{-1} as mentioned in Chapter 2. The output spectrum in Figure 3.7 shows the generation of the second Stokes wave at 1320nm corresponding to the Raman shift ~910cm^{-1}. Note that in the spectrum, the vertical scale is in dB, meaning that each difference in height by 10dB corresponds to 10 times in intensity. If there is 20dB difference, then the higher one has the intensity 100 times larger than that of the lower one.

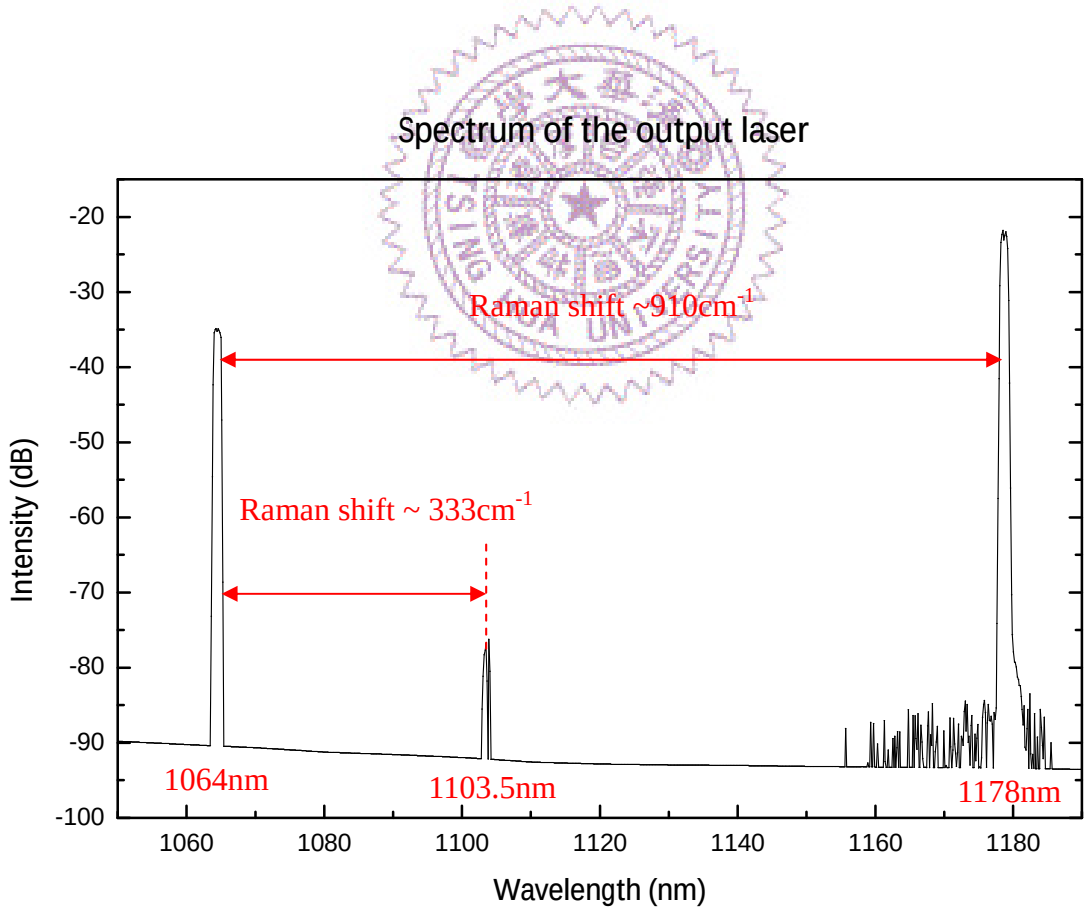

Figure 3.6 This figure shows the spectrum when the first Stokes wave corresponding to the Raman shift of ~333cm^{-1}at 1103.5nm was generated.

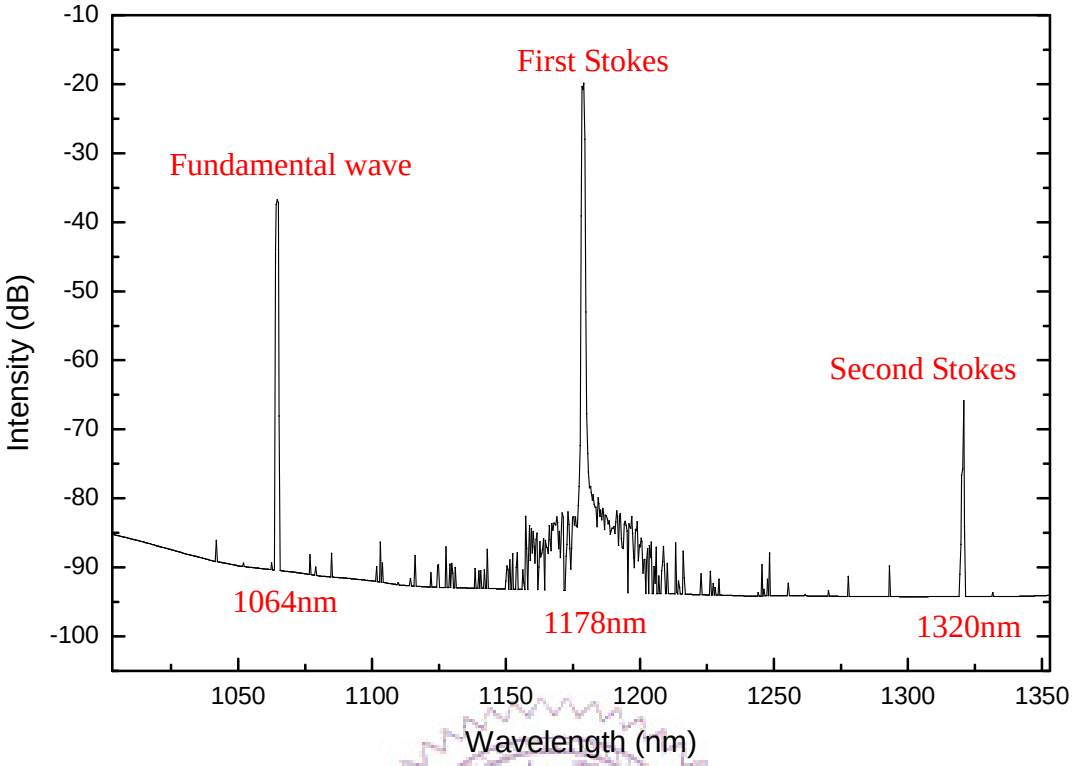

Figure 3.7 This figure shows the spectrum when the second Stokes wave corresponding to the Raman shift of 910cm^{-1} at 1320nm was generated.

The generation of 1103.5nm wave means some intracavity power of 1064nm was wasted. However, since the intensity of 1103.5nm wave was much weaker than that of others, we may not be worry about this. On another hand, the generation of the second Stokes wave means the degradation of the performance of 1178nm, since some 1178nm photons were transformed into second Stokes photons. This phenomenon can be avoided by careful design of the coatings on cavity mirrors to improve the performance of the output laser.

We measured the average output power at 1178nm with respect to the pump power. Note that the error bars in Figure 3.8 mean that the output power in a fixed condition varied with time; the variation was within a range indicated by the error bar.

The hollow point means the center point, and I regard it as the average value. It was found that the variation was mainly due to the setup of $CaWO_4$, which was placed on a mount with a long horizontal rod as shown in Picture 3.1. The little vibration of the

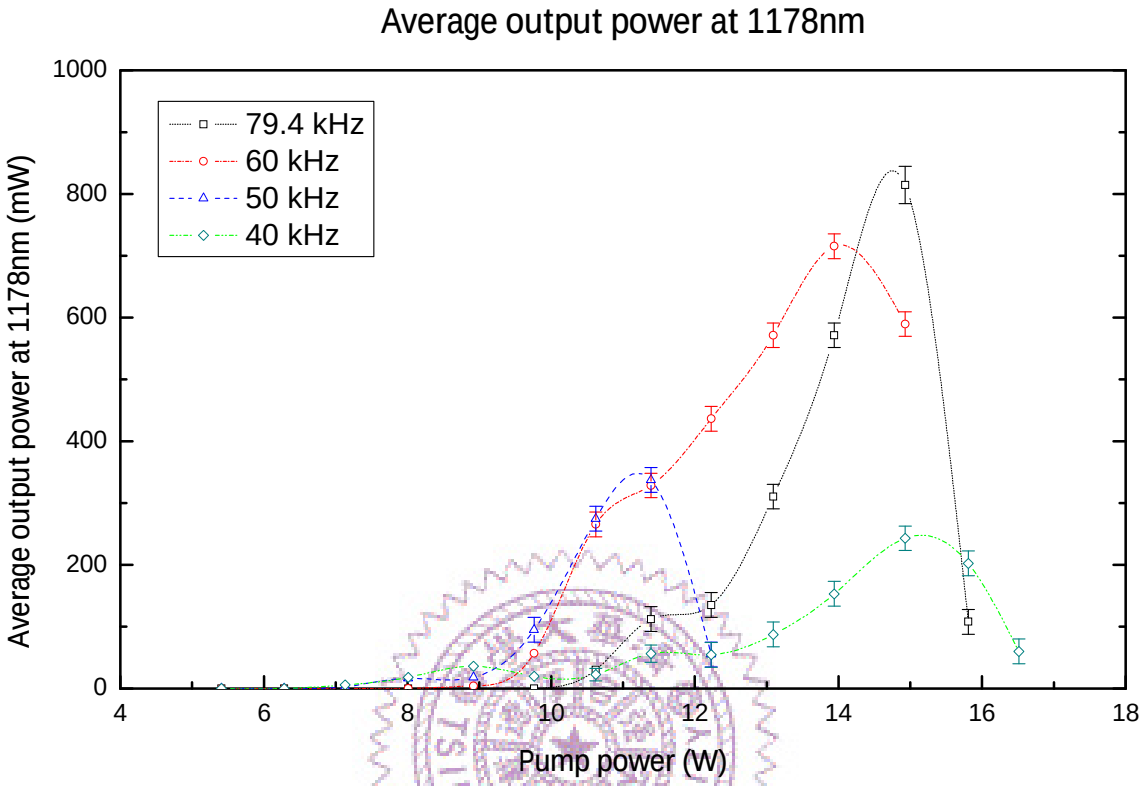

Figure 3.8 The measured average output power at 1178nm with respect to the pump power

long rod resulted in this instability.

From Figure 3.8, we find that the Raman lasing threshold is lower at a lower pulse repetition rate. This is because operation at a lower pulse repetition rate generally gives rise to a higher pulse energy, a shorter pulse width, a higher peak power, and a higher peak intracavity intensity. Measurement of theses physical parameters will be reported in the following. In Figure 3.8, we can thus find that at a fixed pump power, usually a lower pulse repetition rate results in a higher average output power. However, statements just addressed hold provided that the thermal loading or the second Stokes generation has not yet degraded the laser output significantly. From the measured data, we find that each curve at a fixed pulse

repetition rate actually drops down after some critical pump power, and that this critical pump power is higher if the pulse repetition rate is higher. Although a lower pulse repetition rate generally results in a lower Raman lasing threshold and a higher average output power compared with that of a higher pulse repetition rate at the same pump power, the average output power at a lower pulse repetition rate gets saturated more easily and drops suddenly after a lower critical pump power. We can find that generally the available maximum average output power is higher if the laser is operated in a higher pulse repetition rate.

The possible reasons for these observations is that a lower pulse repetition rate results in more severe thermal loading or thermal lensing, and therefore turns the cavity into unstable region as well as degrades the spatial overlapping between the cavity modes of the fundamental and Stokes waves. The dependence on the pulse repetition rate may be due to the energy-transfer up-conversion (ETU) process; it has been studied in [37]. Another possible reason is that the generation of the second Stokes wave is easier at a lower pulse repetition rate such that the output average power of the first Stokes wave is degraded. Therefore the available maximum average output power is generally higher at a higher pulse repetition rate because of less thermal loading and the second Stokes wave; this statement holds provided that the nonlinear drive is sufficient to generate the first Stokes wave, because peak intracavity intensity is lower at a higher pulse repetition rate with a fixed pump power before thermal loading affects the system significantly. Other similar results observed by others can be found in [7] [8] [15] [50] [51] [52] [53].

Note that at each curve with a fixed pulse repetition rate, the maximum average output power drops suddenly after just adding 1A current to the diode laser. It does not have a trend of being flat and then dropping gradually after the critical power, that is, it does not have an obvious region of getting saturation. When the power drops

suddenly, it will be shown later that usually the coating and the crystal surface are damaged. This means that the crystal has to be aligned again.

Note that as for the case of 40kHz, the trend of the corresponding curve seems to be inconsistent with the possible reasons mentioned above. In the cases of the four pulse repetition rates we adopted, it was expected to achieve its available maximum output power at the lowest pump power, and then drop suddenly at the lowest pump power. The possible explanation for this inconsistency is that the data for the case of 40kHz were measured after the damage occurred but without changing the location of the crystal and aligning again.

The measurement of the physical parameters in the last paragraph is reported as follows. The lasing threshold measurement is shown in Table 3.3. Note that the real threshold pump power may not be the value shown in the table, since we cannot continuously tune the pump power. For example, the real threshold pump power is between 8.92W and 9.76W in the case of 79.4kHz.

Pulse repetition rate / Threshold pump Power	79.4 kHz	70 kHz	60 kHz	50 kHz	40 kHz
13A, 6.28W					√
14A, 7.13W				√	
15A, 8.01W			√		
16A, 8.92W		√			
17A, 9.76W	√				

Table 3.3 The table shows the Raman lasing threshold at different pulse repetition rates

In the following, we measured the temporal behaviors of 1064nm and 1178nm pulses by using a grating for separating the two signals.

Figure 3.9 shows the average FWHM pulse width of 1178nm with respect to the pump power.

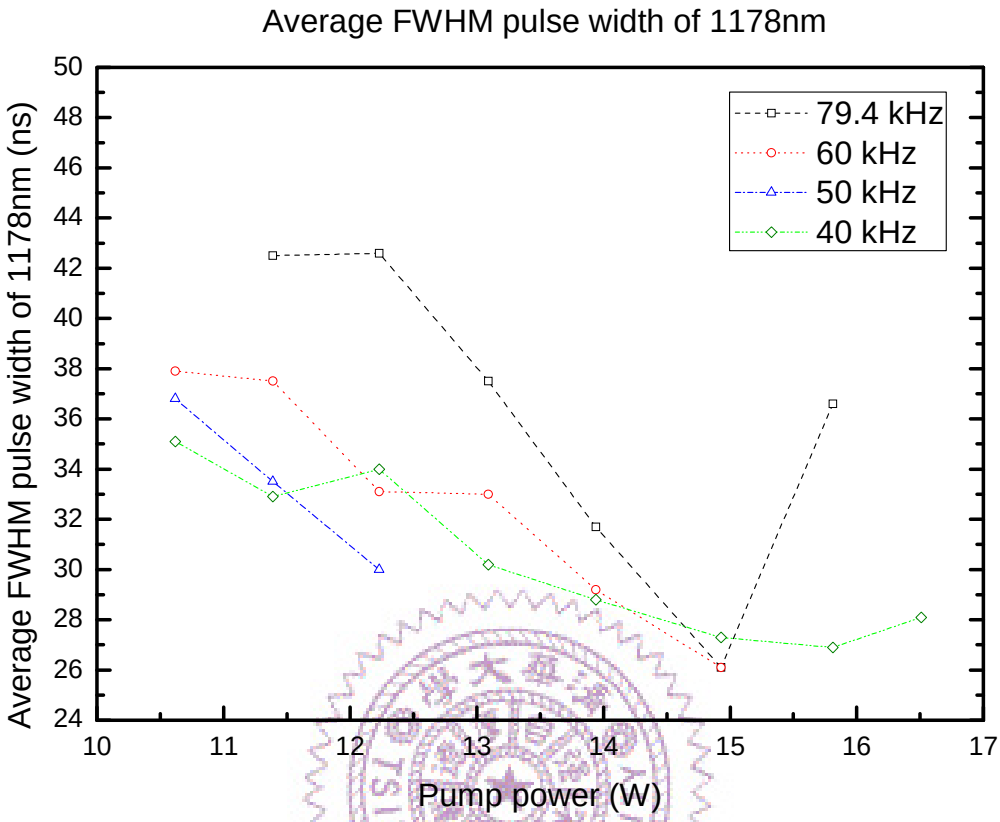

Figure 3.9 The average FWHM pulse width of 1178nm with respect to the pump power

From the measurement, we see that the FWHM pulse width generally becomes larger if the pulse repetition rate is tuned to higher values. The occurring of the exceptions at some pump powers is due to the severe thermal loading and the generation of the second Stokes wave at lower pulse repetition rates. As for the case of 40kHz, data after 12.5W were not recorded, because from Figure 3.8 we knew that the laser was operated over the critical pump power, meaning that damage of the coating or the crystal surface of $CaWO_4$ might easily occur. The situation in each curve is alike. Note that after the critical pump power in each curve, the average output power drops and the pulse width is found to be larger as for the case of 79.4kHz and 40kHz.

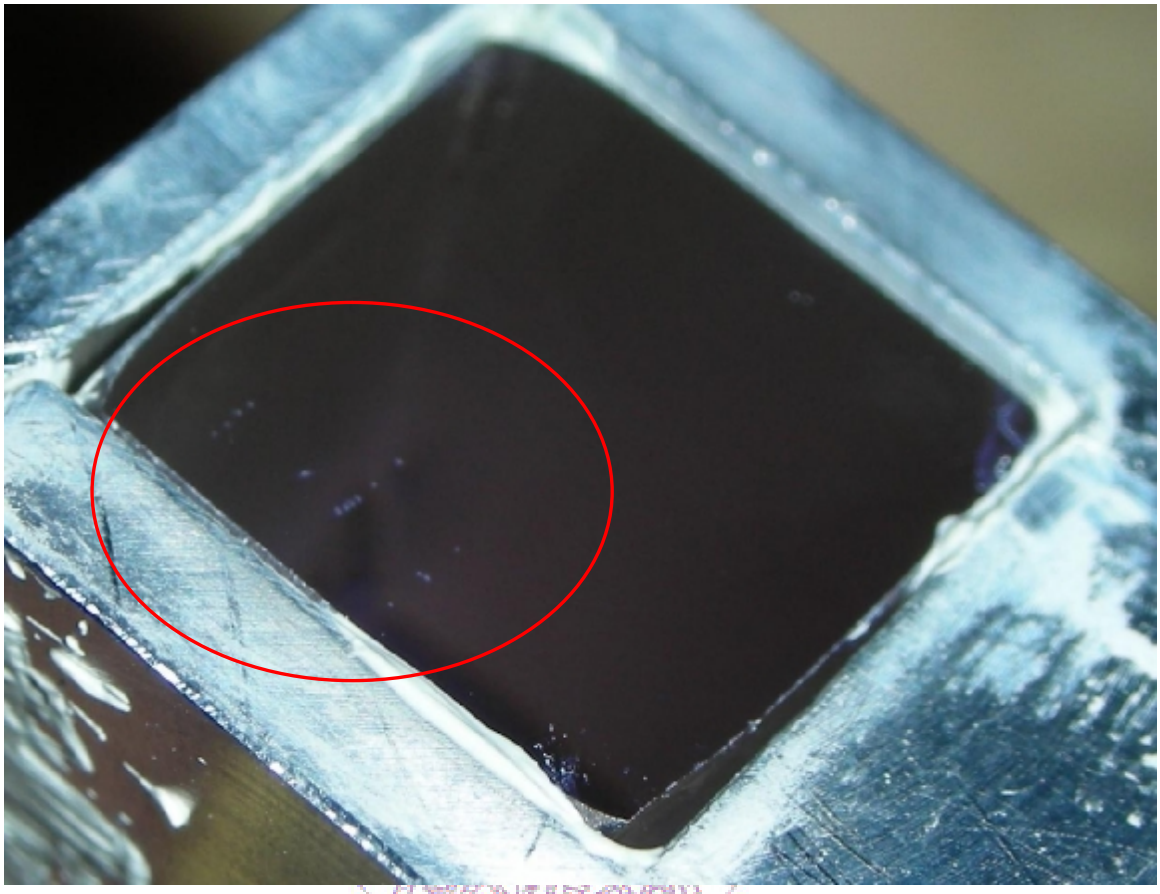

Picture 3.3 Damage on the coating and the crystal surface of $CaWO_4$ under lower pulse repetition rates with a fixed pump power or higher pump powers with a fixed pulse repetition rate

The above picture shows the damage on the coating and the crystal surface of $CaWO_4$ taken under lower pulse repetition rates with fixed pump power or higher pump powers with fixed pulse repetition rate. The generation of the second Stokes wave generally occurs in the similar conditions.

In the following, we will show the measured temporal behaviors observed from the oscilloscope with 500MHz bandwidth connected to a fast silicon detector. By dividing the average output power at 1178nm by the pulse repetition rate, we can get the average pulse energy as shown in Figure 3.10 by assuming regular pulse trains. By dividing the average pulse energy by the FWHM pulse width, we can get the average peak power as shown in Figure 3.11.

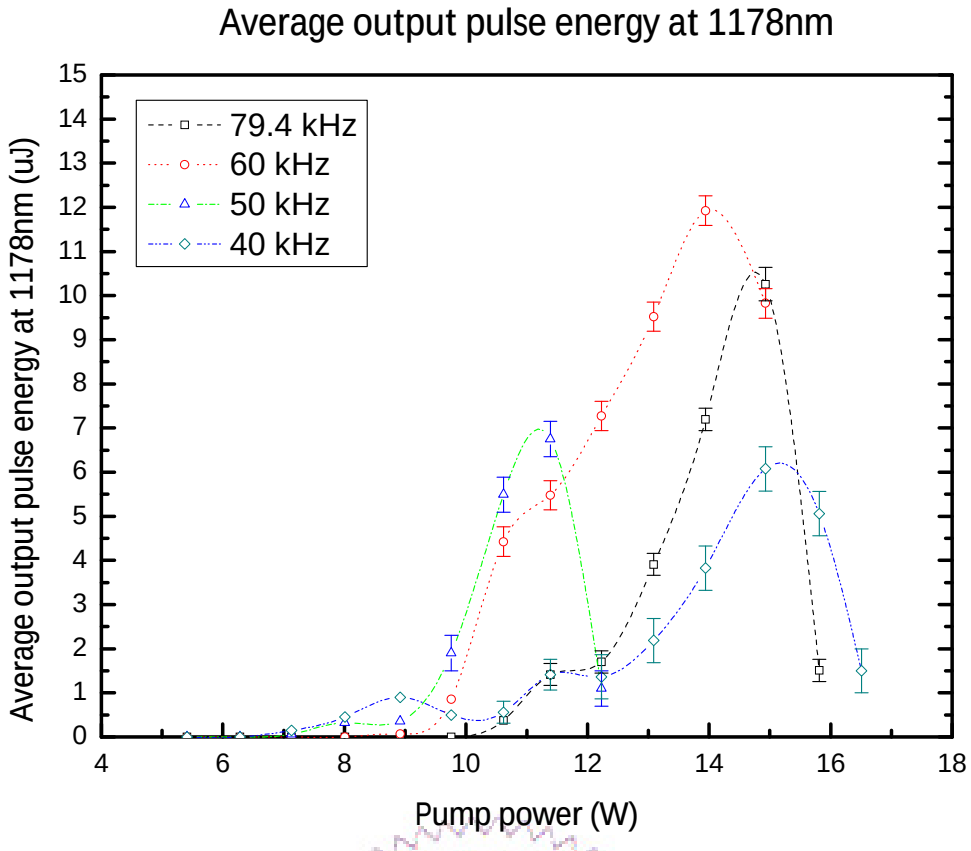

Figure 3.10 The calculated average output pulse energy of 1178nm with respect to the pump power

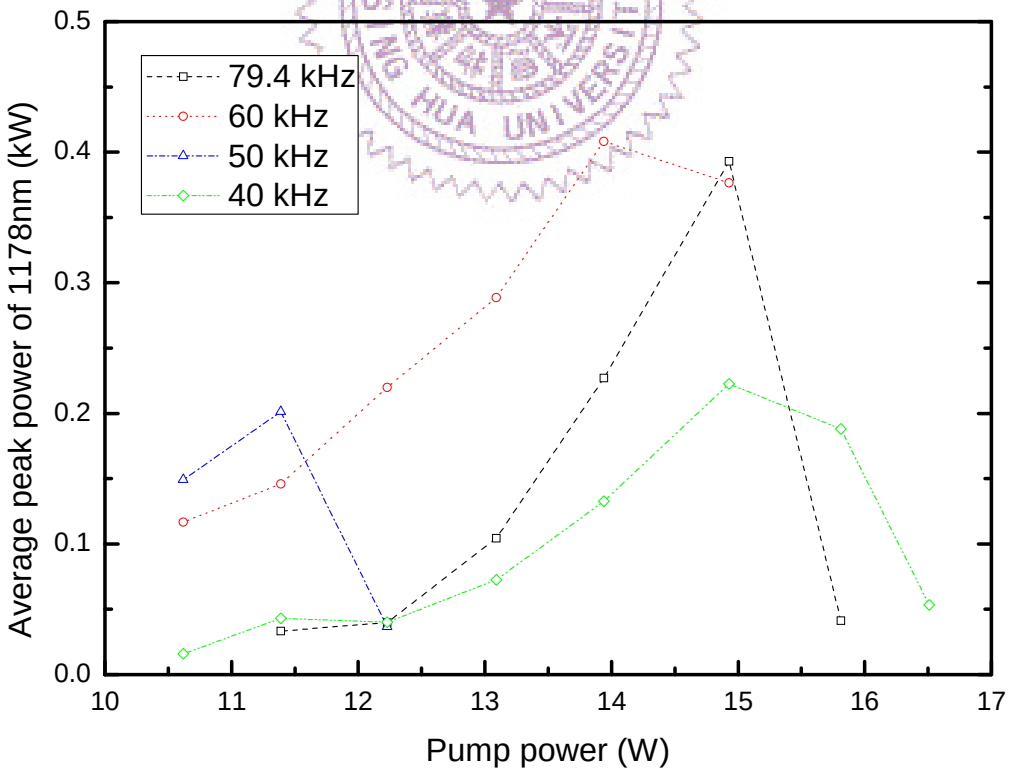

Figure 3.11 The calculated average peak power of 1178nm with respect to the pump power

The above two figures support the statements which explain the experimental results.

Figure 3.12 below shows the pulse widths and pulse trains of 1064nm or 1178nm at pulse repetition rate of 79.4kHz viewed from the screen of the oscilloscope.

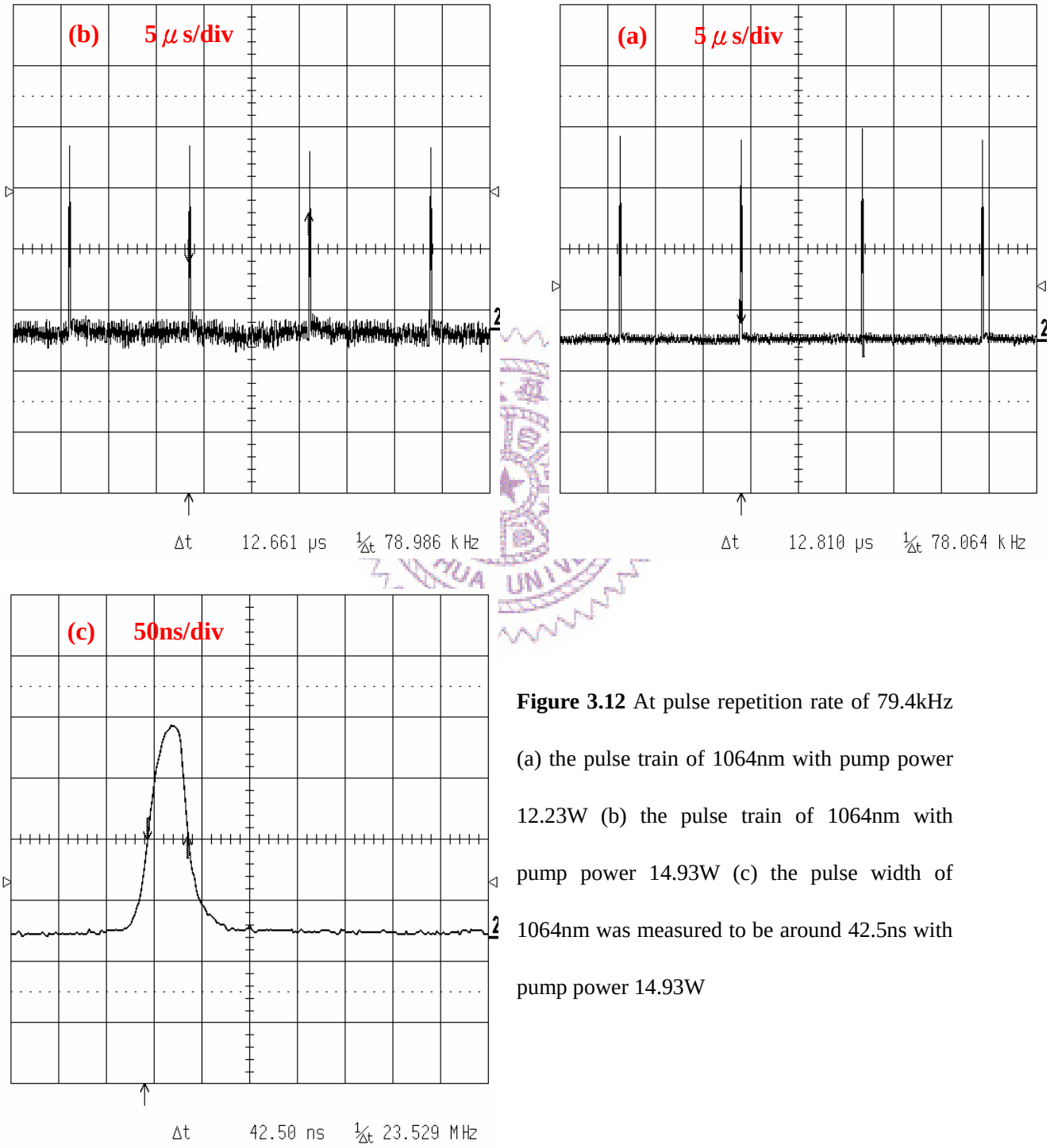

Figure 3.12 At pulse repetition rate of 79.4kHz (a) the pulse train of 1064nm with pump power 12.23W (b) the pulse train of 1064nm with pump power 14.93W (c) the pulse width of 1064nm was measured to be around 42.5ns with pump power 14.93W

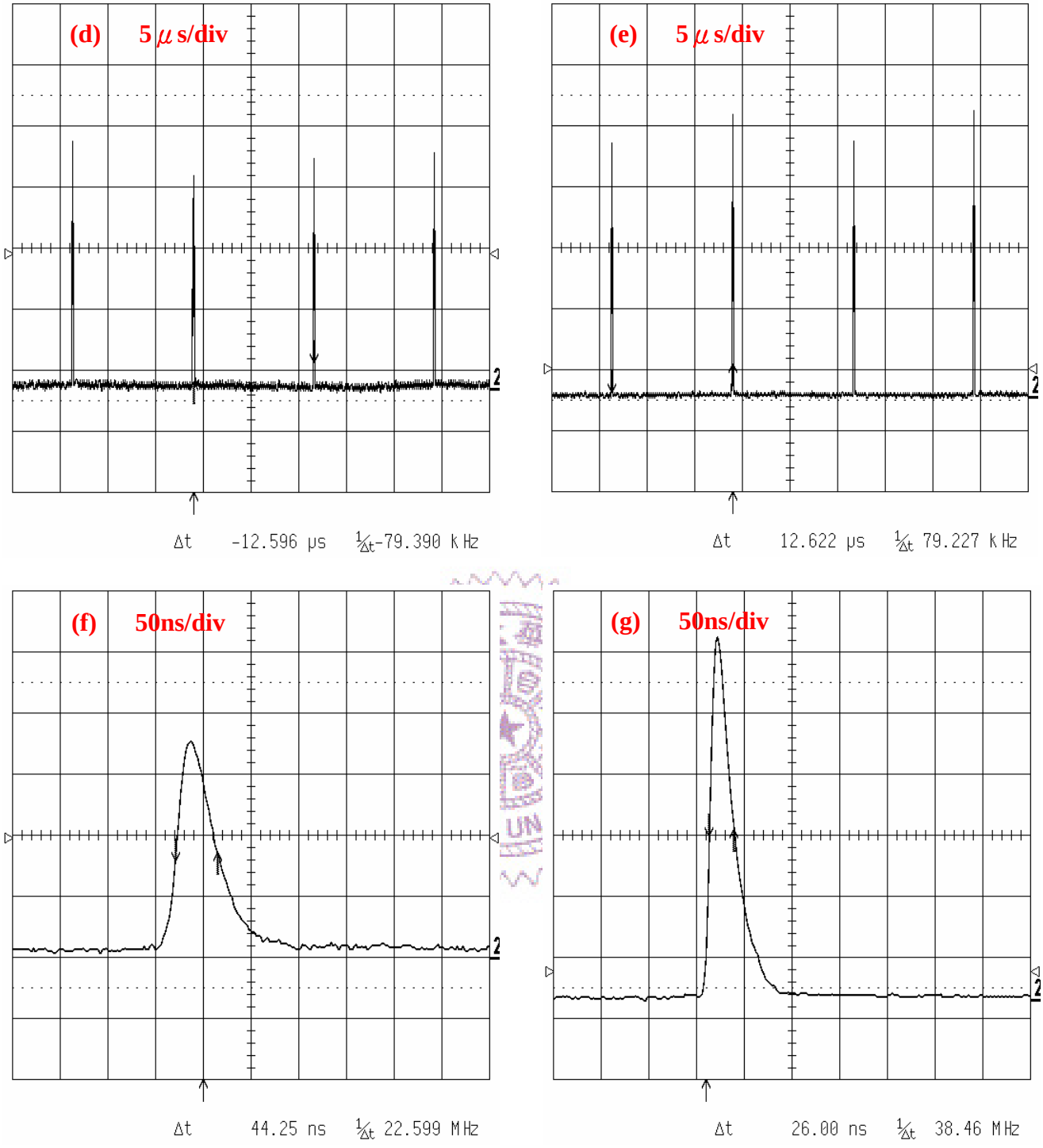

Figure 3.12 At pulse repetition rate of 79.4kHz (d) the pulse train of 1178nm with pump power 12.23W (e) the pulse train of 1178nm with pump power 14.93W (f) the FWHM pulse width of 1178nm was measured to be around 44.25ns with pump power 12.23W (g) the FWHM pulse width of 1178nm was measured to be around 26ns with

pump power 14.93W.

Figure 3.13 below shows the pulse widths and pulse trains of 1064nm or 1178nm at pulse repetition rate of 40kHz viewed from the screen of the oscilloscope.

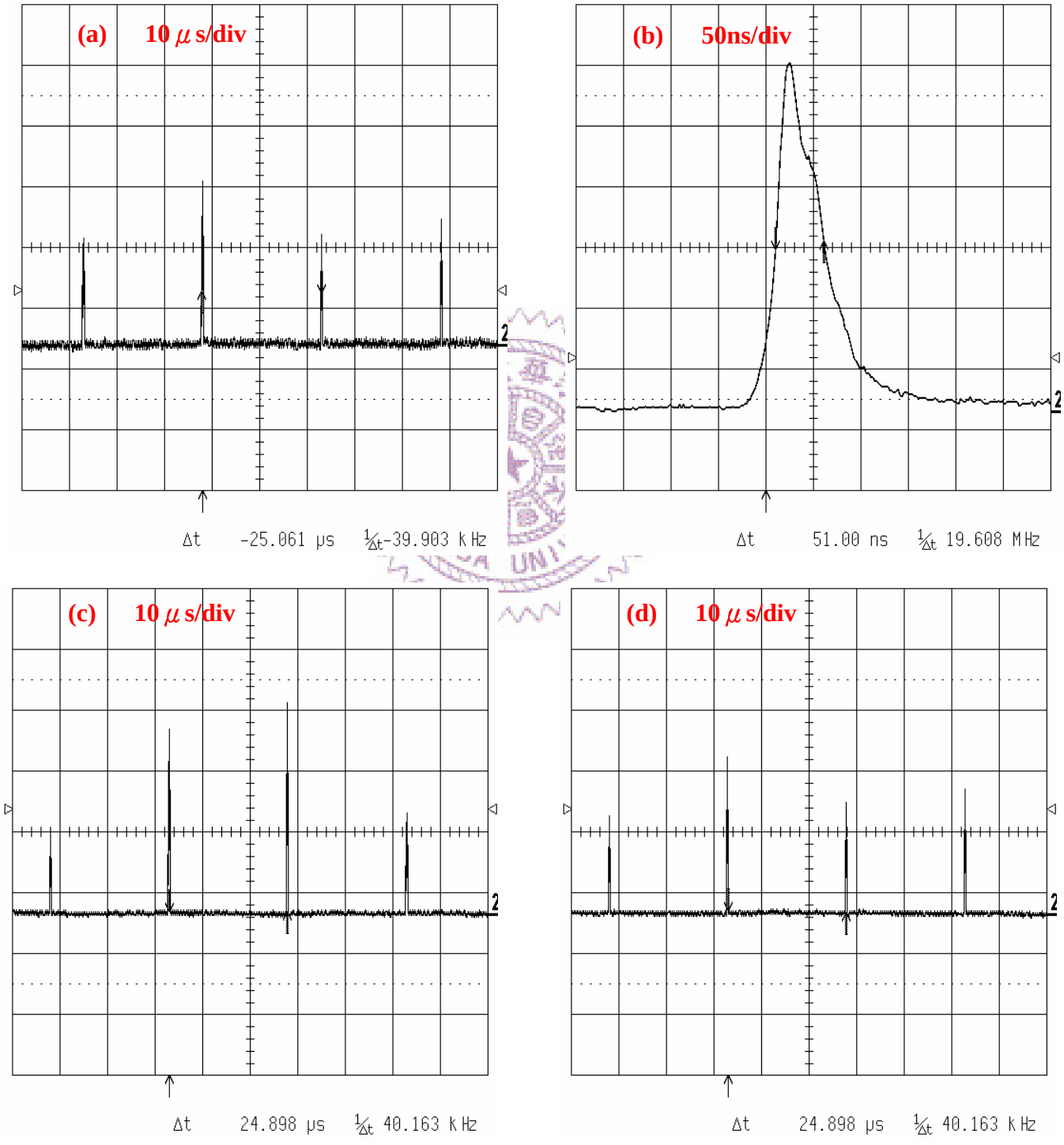

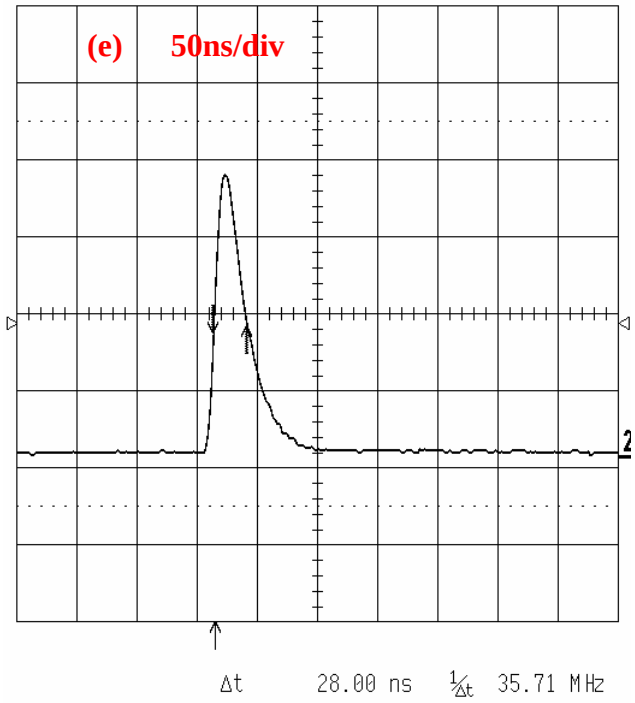

Figure 3.13 At pulse repetition rate of 40kHz (a) the pulse train of 1064nm with pump power 14.93W (b) the FWHM pulse width of 1064nm was measured to be around 51ns with pump power 14.93W (c) the pulse train of 1178nm with pump power 14.93W (d) the pulse train of 1178nm with pump power 14.93W taken at another time shot (e) the FWHM pulse width of 1178nm was measured to be around 28ns with pump power 14.93W

Figure 3.12 and 3.13 show the pulse trains and the pulse shapes of 1064nm and 1178nm, letting us know the temporal differences between 1064nm and 1178nm at some pulse repetition rate, and the differences in temporal behaviors between higher and lower pulse repetition rates. From either Figure 3.12 or 3.13, we find that the pulse train of 1064nm is more regular and stable than that of 1178nm. The reason may be the little instability resulted from the mount of $CaWO_4$ as mentioned before. On the other hand, we can see that the pulse trains of 1064nm and 1178nm are more stable and regular at 79.4kHz than that at 40kHz. This is because the thermal loading is more severe at 40kHz.

In the following, investigation of the spectrum before and after adding M3 is shown in the next page.

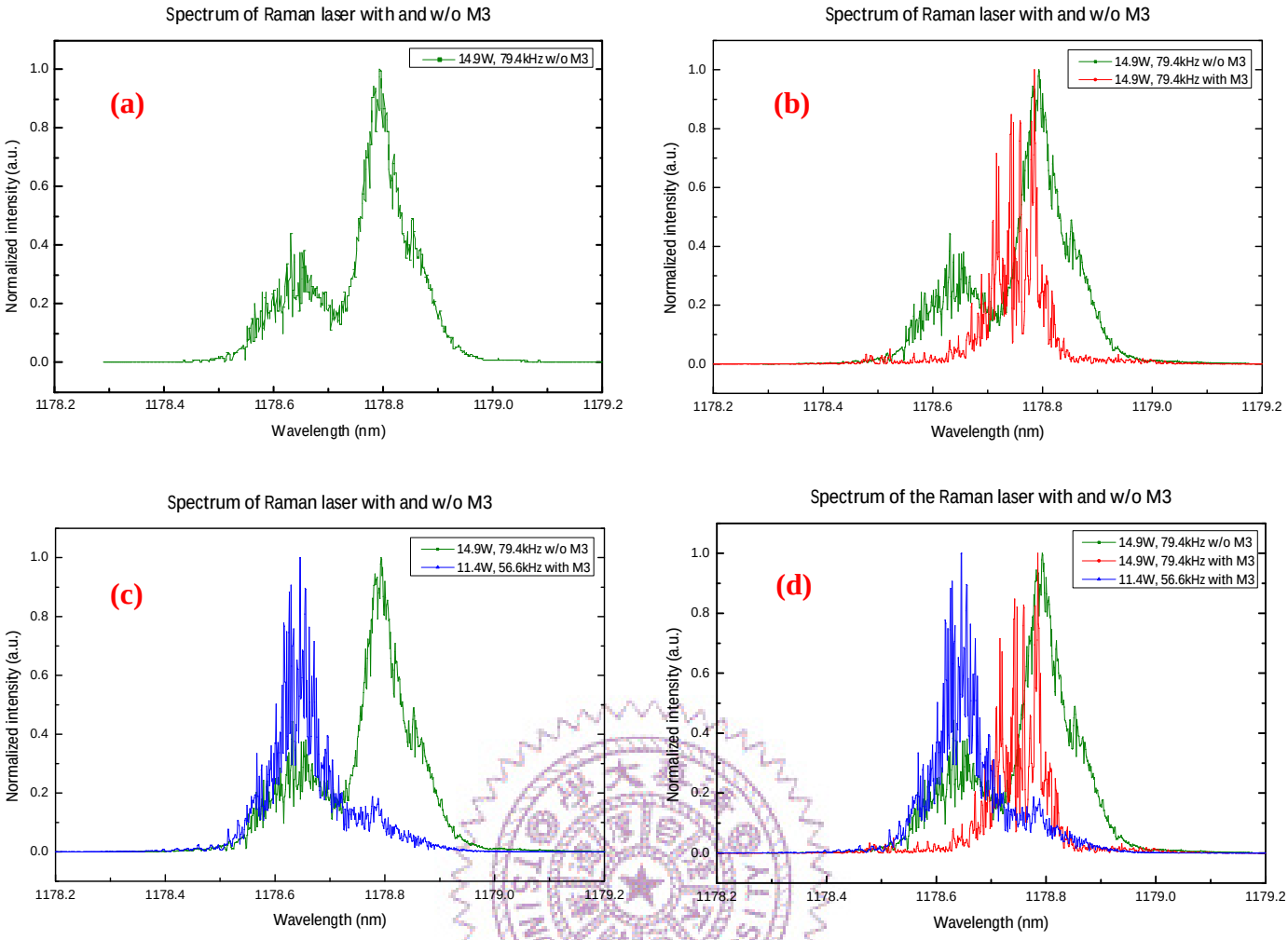

Figure 3.14 (a) the green curve is the 1178nm spectrum at 79.4kHz with pump power of 14.9W and without M3 (b) the red curve is the 1178nm spectrum at 79.4kHz with pump power of 14.9W and with M3 added (c) the blue curve is the 1178nm spectrum at 56.6kHz with pump power of 11.4W and with M3 added (d) the composite spectrum for comparison

In Figure 3.14(a), the spectral hole burning in the spectrum of the first Stokes wave may be resulted from the generation of the second Stokes wave. However, this explanation has not yet been confirmed by the experiment. From Figure 3.14, we see that the linewidth of 1178nm was narrowed down to around 0.1nm after adding M3. Note that when the pump power was changed from 14.9W to 11.4 W with other conditions unchanged, the peak of the spectrum was shifted. By tuning the pulse repetition rate, we found that the location of the peak did not shift in the spectrum, and the intensity in the spectrum was maximum at 56.6kHz. However, I do not

exactly know the mechanism behind the shift of the peak. Also note that the intensity of each colored curve is normalized to one for comparison of the linewidth.

Some reported linewidth of the yellow laser are summarized below.

1. 0.2nm linewidth at CW 1178nm in a "narrow-line, 1178nm CW bismuth-doped fiber laser with 6.4W output for direct frequency doubling "(April 2007). [13]
2. 0.1~0.37nm linewidth at CW 1178nm; 0.25nm linewidth at 589nm in a "Watts-level frequency doubling of a narrow line linearly polarized Raman fiber laser to 589 nm" (September 2005). [14]
3. 13GHz linewidth at pulsed 589nm in "Generation of tunable 589nm radiation as a Na guide star source using an optical parametric amplifier" (January 2009). [11]

Before doing the experiment in the configuration with a grating feedback, I intended to do intracavity SHG in this linear cavity without adding M3 and replace M2 by M4 to get some feeling about the change in the cavity mode and experiences in intracavity SHG. The following is the real experimental setup.

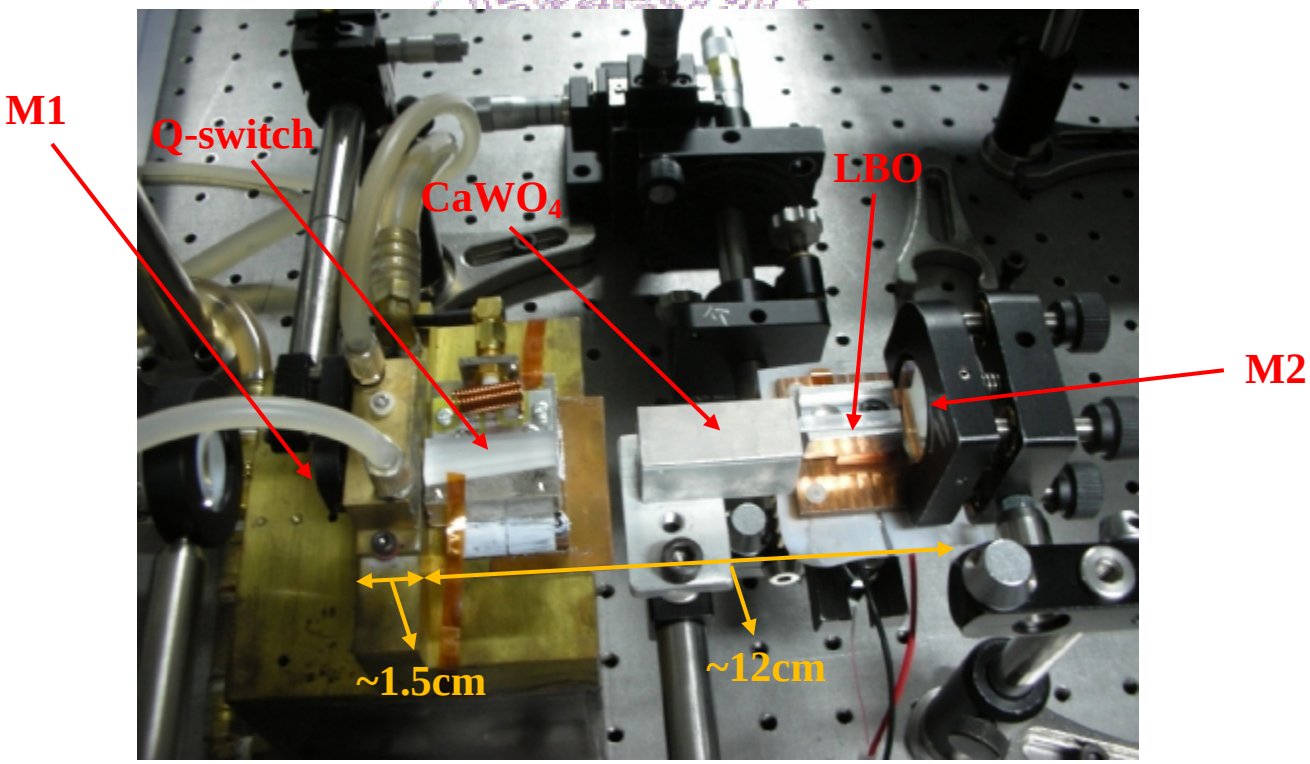

Picture 3.4 The real experimental setup for doing intracavity SHG in the linear cavity

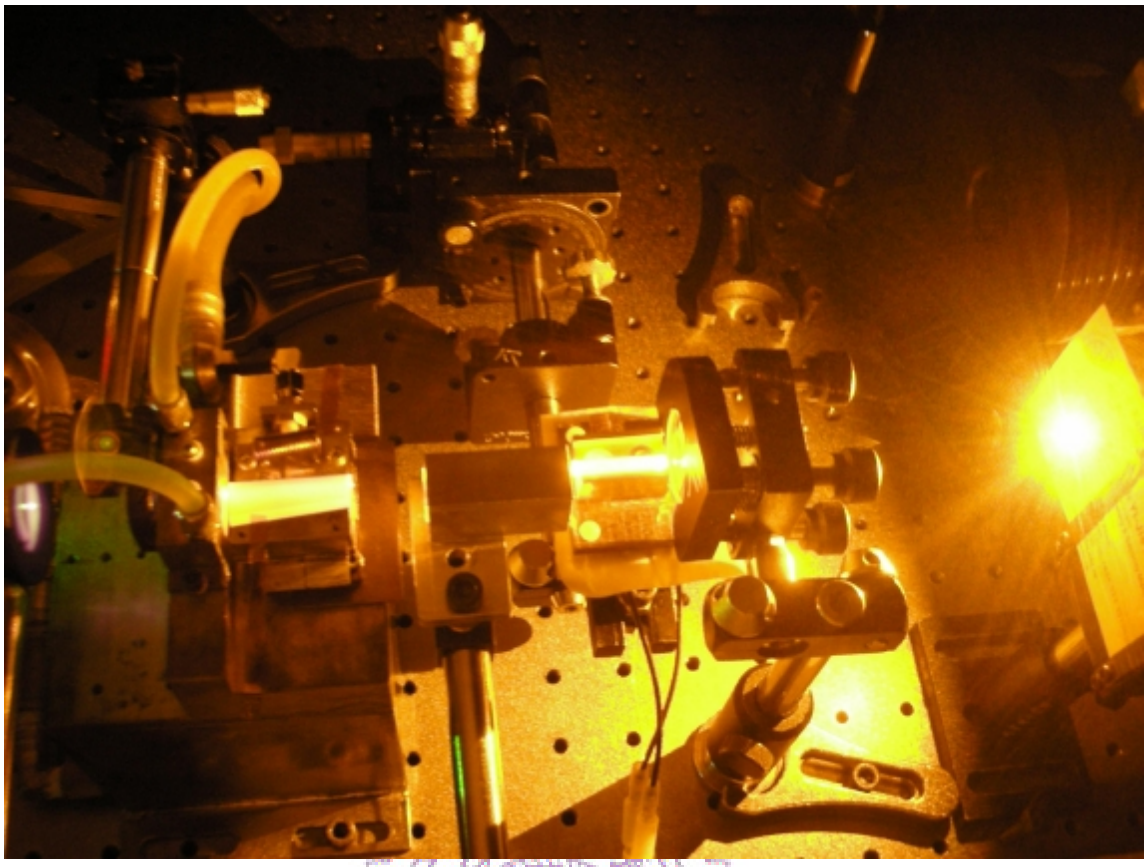

Picture 3.5 (a) the generation of the sodium-yellow laser by doing intracavity SHG

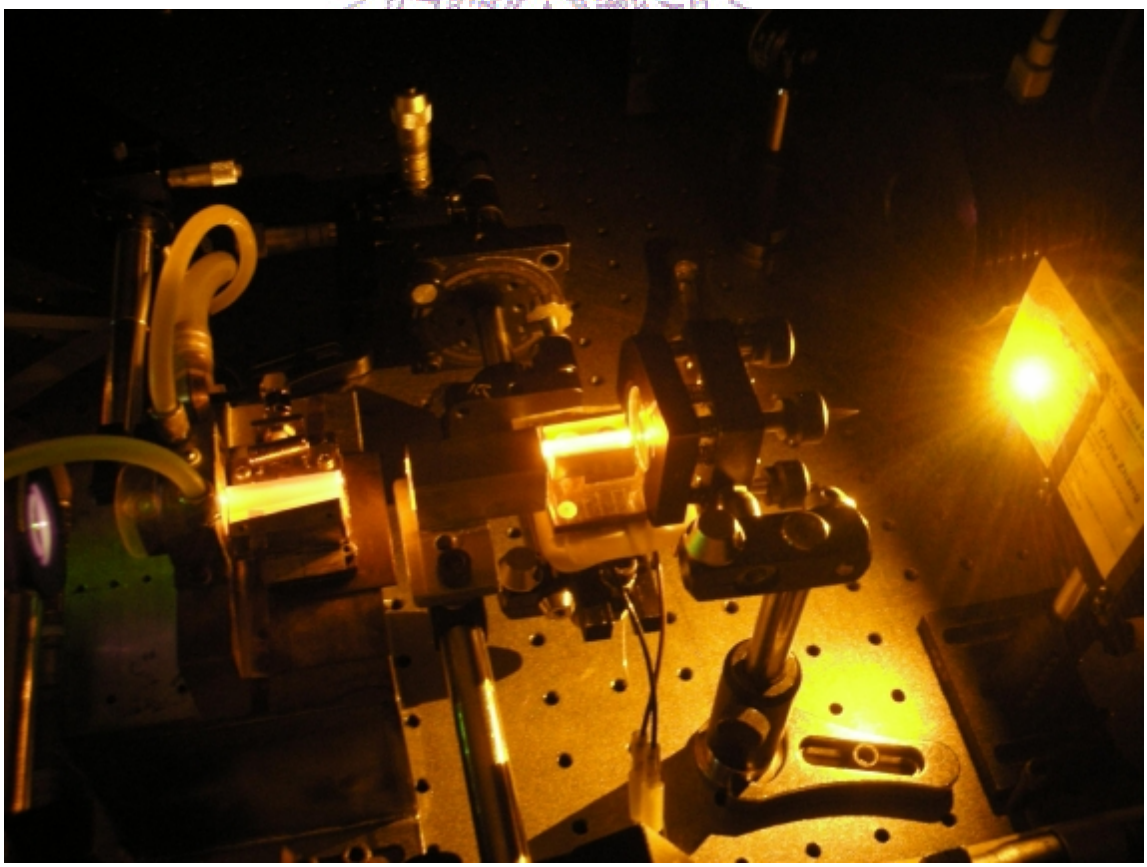

Picture 3.5 (b) the generation of the sodium-yellow laser by doing intracavity SHG

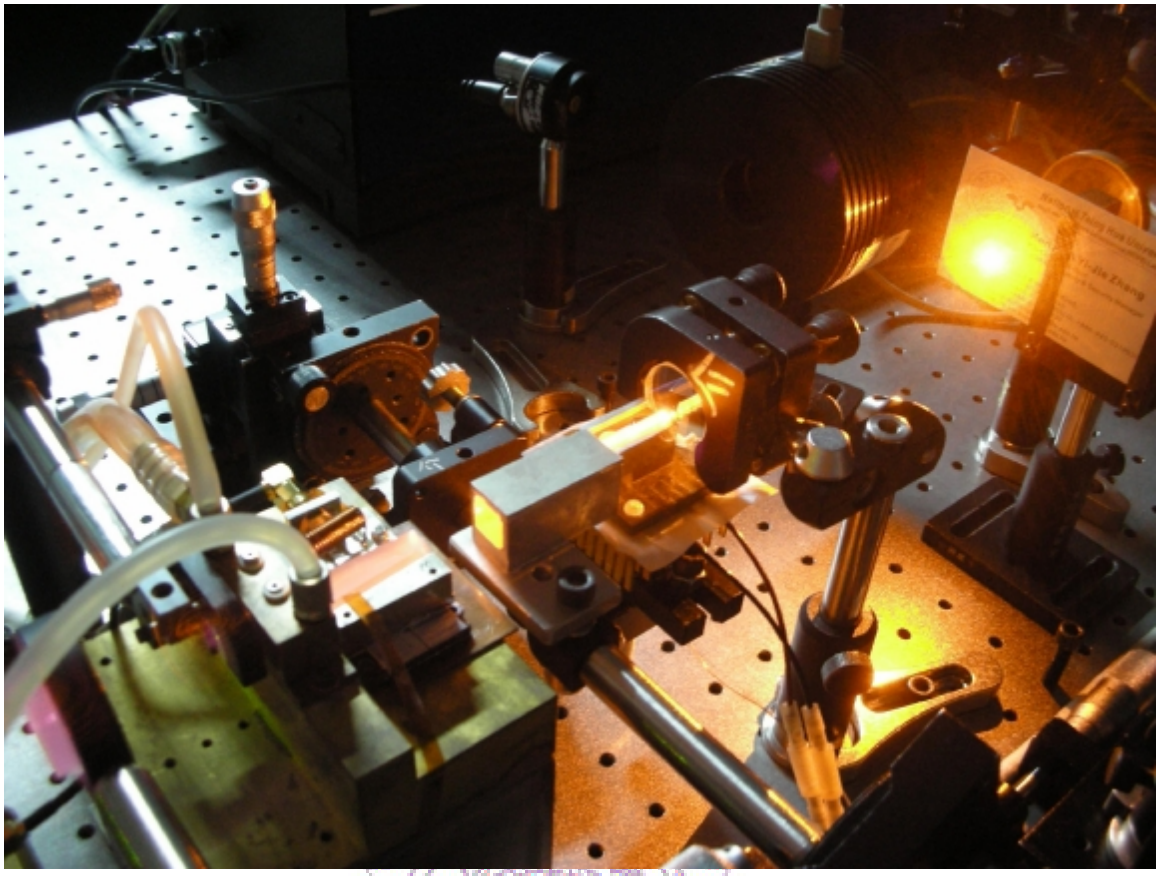

Picture 3.5 (c) the generation of the sodium-yellow laser by doing intracavity SHG

The three pictures above show the generation of the sodium-yellow laser by doing intracavity SHG. From the picture we found that the sodium-yellow laser was operated at the fundamental transverse mode. The maximum average power was obtained around 130mW measured from M4. If assuming that equal power is generated in forward and backward directions, the maximum total average power generated is estimated to be around 350mW under Pump power: ~ 18W. The diode to yellow conversion efficiency is around 2%. However, since the cavity alignment was not optimized, and the coating on the LBO crystal used in this experiment is:

S1: R=2.0279%@1064nm

S2: R=1.6404%@1064nm

R<0.3%@1178nm

R<0.5%@589nm

I expect that the average output power can be improved by using LBO with proper coating and after empirical optimization.

3.5.2 Raman Laser with a Grating Feedback

The experiment about this part is still under way. Currently, the oscillation of both 1064nm and 1178nm in the folded cavity has been achieved. I have been trying to set up a grating feedback and doing some measurements. The results will be reported after the experiment is done.

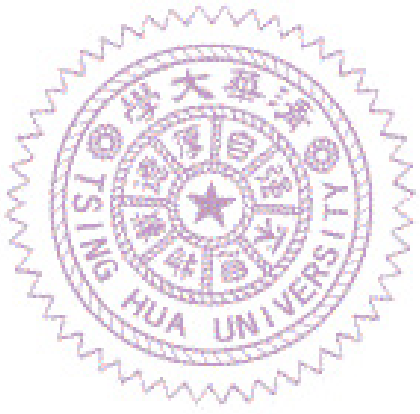

Chapter 4 Conclusions and Future Works

In summary, two methods are proposed to narrow down the laser output linewidth. Specifically, it needs more careful calculations for a cavity with an etalon coupler such that the effectiveness and feasibility can be estimated and compared with the experiment. In our experiment, linewidth of around 0.1nm at 1178nm was achieved in a linear cavity configuration with an etalon coupler. As for the folded cavity with a grating feedback, it looks promising and more reliable. However, the experiment is still under way.

In the future, we will investigate and study the folded cavity with a grating feedback systematically. As for this part, we want to know the effectiveness of grating feedbacks from 1178nm and 1064nm waves. In particular, we would like to know the effect of the grating feedback from either or both of the 1064-nm and 1178-nm components. Additionally, the output coupler of this kind of configuration might be replaced by a partial reflector to optimize the average output power for extracavity SHG. With this scheme, the cavity length is shorter, and the laser system could be operated in higher pump powers to achieve a larger output power for the yellow laser. The results can be compared with that of the original folded cavity which is designed for intracavity SHG.

It seems that the Raman crystal has to be polished and coated again in the future because of the damage on the crystal.

As for a CW Raman laser based on $CaWO_4$, calculation for the feasibility has to be done before we proceed with the experiment. Suitable optics and a careful cavity design are also needed.

References

[1] Craig A. Denman et al, “20 W CW 589 nm sodium beacon excitation source for adaptive optical telescope applications”, Optical Materials, 26 (2004) 507–513

[2] Joseph D. Vance et al, “Continuous-wave, all-solid-state, single-frequency 400-mW source at 589 nm based on doubly resonant sum-frequency mixing in a monolithic lithium niobate resonator”, Applied Optics, Vol. 37, No. 21, 20 July 1998

[3] Yan Feng et al, “589nm Light Source Based on Raman Fiber Laser”, Japanese Journal of Applied Physics, Vol. 43, No. 6A, 2004

[4] Jirí Janousek et al, “Efficient all solid-state continuous-wave yellow orange light source”, Optics Express, Vol. 13, No. 4, 21 February 2005

[5] Peter Dekker et al, “All-solid-state 704mW continuous-wave yellow source based on an intracavity, frequency-doubled crystalline Raman laser”, Optics Letters, Vol. 32, No. 9 / May 1, 2007

[6] P. H. Chiu et al, “All-solid-state single-mode sum-frequency generation of sodium resonance radiation”, Optics Letters, Vol. 19, No. 24 / December 15, 1994

[7] Peter Dekker et al, “Continuous-wave, intracavity doubled, self-Raman laser operation in Nd:$GdVO_4$ at 586.5nm”, Optics Express, Vol. 15, No. 11, 28 May 2007

[8] Shutao Li et al, “Diode-side-pumped intracavity frequency-doubled Nd:YAG/$BaWO_4$ Raman laser generating average output power of 3.14 W at 590 nm”, Optics Letters, Vol. 32, No. 20, October 15, 2007

[9] Richard P. Mildren et al, “Discretely tunable, all-solid-state laser in the green, yellow, and red”, Optics Letters, Vol. 30, No. 12 / June 15, 2005

[10] H. M. Pask and J. A. Piper, “Efficient all-solid-state yellow laser source producing 1.2-W average power”, Optics Letters, Vol. 24, No. 21 / November 1, 1999

[11] Malte Duering et al, “Generation of tunable 589nm radiation as a Na guide star source using an optical parametric amplifier”, Optics Express, Vol. 17, No. 2, 19 January 2009

[12] Yan Feng et al, “Multiple-color cw visible lasers by frequency sum-mixing in a cascading Raman fiber laser”, Optics Express, Vol. 12 No. 93, May 2004

[13] A. B. Rulkov1 et al, “Narrow-line, 1178nm CW bismuth-doped fiber laser with 6.4W output for direct frequency doubling”, Optics Express, Vol. 15, No. 9, 30 Apr 2007

[14] D. Georgiev et al, “Watts-level frequency doubling of a narrow line linearly polarized Raman fiber laser to 589 nm,” Optics Express, Vol. 13, No. 18, September 2005

[15] James T. Murray et al, “End-pumped intracavity solid state Raman lasers”, Advanced Solid State Lasers, OSA TOPS Vol. 19, 1998

[16] T. H. Jeys et al. in Conference on Lasers and Electro-Optics (Optical Society of America, Washington, D.C., 1987), paper WE6.

[17] Robert L. Byer, “Diode laser-pumped Solid-State Lasers”, Science, Vol.239, 12 February 1998

[18] W. Koechner, “Solid-State Laser Engineering”, Sixth Revised and Updated Edition, Springer Series in OPTICAL SCIENCES

[19] W. Koechner, “Solid-State Laser Engineering”, page 54, Sixth Revised and Updated Edition, Springer Series in OPTICAL SCIENCES

[20] W. Koechner, “Solid-State Laser Engineering”, page 72,73, Sixth Revised and Updated Edition, Springer Series in OPTICAL SCIENCES

[21] H. M. Pask, “The design and operation of solid-state Raman lasers”, Progress in Quantum Electronics, 27 (2003) 3-56

[22] http://en.wikipedia.org/wiki/Raman_scattering

[23] Singh, Rajinder, "C.V. Raman and the Discovery of the Raman Effect", Physics in Perspective (PIP) **4**: 399. (2002)

[24] Yen-Chieh Huang, “Principles of Nonlinear Optics”, course reader in the course “Nonlinear Optics” in National Tsing Hua University

[25] http://www.rp-photonics.com/raman_scattering.html

[26] Charles Kittel, “Introduction to Solid State Physics”, Eighth Edition, Wiley

[27] H. M. Pask, “Continuous-wave, all-solid-state, intracavity Raman laser”, Optics Letters, Vol. 30, No. 18, September 15, 2005

[28] L. Fan et al, “Continuous-wave intracavity Raman laser at 1179.5nm with $SrWO_4$ Raman crystal in diode-end-pumped Nd:YVO_4 laser”, Applied Physics B, 2009

[29] Saleh and Teich, “Fundamentals of Photonics”, chapter 19, First Edition, Wiley

[30] YC. Huang and R.L. Byer, report on “Raman gain measurement for Calcium Tungstate”, September 8, 1995

[31] Alexander A. Kaminskii et al, “Properties of Nd^{3+}-doped and undoped tetragonal $PbWO_4$, $NaY(WO_4)_2$, $CaWO_4$, and undoped monoclinic $ZnWO_4$ and $CdWO_4$ as laser-active and stimulated Raman scattering-active crystals”, Applied Optics, Vol. 38, No. 21, 20 July 1999

[32] M. Bass, Handbook of Optics, McGraw-Hill, New York, 1995

[33] T.T. Basiev et al, Optical Materials 11 (4) (1999) 307–314

[34] T.T. Basiev et al, Applied Optics 38 (3) (1999) 594–598

[35] Datasheet of the vendor, EXCEL OPTRONICS

[36] Datasheet of the vendor, EKSMA OPTICS

[37] Y.P. Lan, Y.F.Chen, S.C.Wang, “Repetition-rate dependence of thermal loading in diode-end-pumped Q-switched lasers: influence of energy-transfer upconversion”, Applied Physics B, 71, 27–31 (2000)

[38] T. Hänsch, Applied Optics, 11, 895, 1972

[39] I. Shoshan et al, “Narrowband operation of a pulsed dye laser without intracavity beam expansion”, Journal of Applied Physics, Vol.48, No.11, November 1977

[40] Michael G. Littman and Harold J. Metcalf, “Spectrally narrow pulsed dye laser without beam expander”, Applied Optics, Vol. 17, No. 14, 15 July 1978

[41] K. C. Harvey and C. J. Myatt, “External-cavity diode laser using a grazing-incidence diffraction grating”, Optics Letters, Vol. 16, No. 12, June 15, 1991

[42] J. E. Bernard et al, “Grating-tuned, single-longitudinal-mode, diode-pumped Nd:YVO_4 laser”, Optics Letters , Vol. 18, No. 23, December 1, 1993

[43] Chi-Sheng Yu and A. H. Kung, “Grazing-incidence periodically poled $LiNbO_3$ optical parametric oscillator”, J. Opt. Soc. Am. B, Vol. 16, No. 12, December 1999

[44] Y. Y. Lin et al, “Single-longitudinal-mode, tunable dual-wavelength, CW Nd:YVO_4 laser”, Optics Express, Vol.14, No.12, 12 June 2006

[45] H. Kogelnik: Bell Syst. Tech. J. **44**, 455 (1965)

[46] W. Koechner, “Solid-State Laser Engineering”, page 232, Sixth Revised and Updated Edition, Springer Series in OPTICAL SCIENCES

[47] W. Koechner, “Solid-State Laser Engineering”, page 233, Sixth Revised and Updated Edition, Springer Series in OPTICAL SCIENCES

[48] W. Koechner, “Solid-State Laser Engineering”, page 477, 478, Sixth Revised and Updated Edition, Springer Series in OPTICAL SCIENCES

[49] Yi-Ying Lai, “High efficiency diode pumped Nd:YAG laser using a needle-thin gain medium”, Master thesis, National Tsing Hua University

[50] Y. F. Chen, “Efficient 1521-nm Nd:$GdVO_4$ Raman laser”, Optics Letters , Vol. 29, No. 22, November 15, 2004

[51] Y. F. Chen et al, “Efficient diode-pumped actively Q-switched Nd:YAG/$BaWO_4$ intracavity Raman laser”, Optics Letters , Vol. 30, No. 24, December 15, 2005

[52] K. W. SU et al, “Power scale-up of the diode-pumped actively Q-switched

Nd:YVO_4 Raman laser with an undoped YVO_4 crystal as a Raman shifter", Applied Physics B , 88, 47-50 (2007)

[53] Kuan-Wei Su et al, "Efficient high-peak-power diode-pumped actively Q-switched Nd:YAG/YVO_4 intracavity Raman laser", Applied Optics, Vol. 47, No. 35, December 10, 2008